

The Chemical Thermodynamics for Growing Systems

Yuki Sughiyama,* Atsushi Kamimura,* Dimitri Loutchko, and Tetsuya J. Kobayashi†

*Institute of Industrial Science, The University of Tokyo,
4-6-1, Komaba, Meguro-ku, Tokyo 153-8505 Japan*

(Dated: January 25, 2022)

We consider growing open chemical reaction systems (CRSs), in which autocatalytic chemical reactions are encapsulated in a finite volume and its size can change in conjunction with the reactions. The thermodynamics of growing CRSs is indispensable for understanding biological cells and designing protocells by clarifying the physical conditions and costs for their growing states. In this work, we establish a thermodynamic theory of growing CRSs by extending the Hessian geometric structure of non-growing CRSs. The theory provides the environmental conditions to determine the fate of the growing CRSs; growth, shrinking or equilibration. We also identify thermodynamic constraints; one to restrict the possible states of the growing CRSs and the other to further limit the region where a nonequilibrium steady growing state can exist. Moreover, we evaluate the entropy production rate in the steady growing state. The growing nonequilibrium state has its origin in the extensivity of thermodynamics, which is different from the conventional nonequilibrium states with constant volume. These results are derived from general thermodynamic considerations without assuming any specific thermodynamic potentials or reaction kinetics; i.e., they are obtained based solely on the second law of thermodynamics.

I. INTRODUCTION

Self-replication is a hallmark of living systems by which they are differentiated from nonliving ones. Since von Neumann's formulation of self-reproducing automata [1, 2], the physical and chemical basis of self-replication has been pursued theoretically and experimentally in order to understand and synthesize living systems [3–24]. Of the various components necessary for self-replication, autocatalytic reaction cycles, thought of as the driving engine, form a central part [25–31]. However, the presence of cycles is not sufficient for self-replication. Because the cycles should be confined in an encapsulating volume which defines the replication unit, the size of the volume should also grow in accordance with the production of chemicals by the cycles.

In spite of the active investigation of autocatalytic reaction cycles in the last decades [25–31], the growth of volume and its coupling with the autocatalytic cycles have not been thoroughly investigated so far. Although the recent rediscovery of growth laws of bacteria [32] initiated a surge of new coarse-grained autocatalytic models [10–12, 33–38], the volume growth in these models is considered only heuristically [5, 39–42], e.g., by representing it with a linear function of chemicals in it.

In the light of chemical thermodynamics, the change in volume and the influx and outflux of chemicals driven by the cycles are mutually dependent and should be thermodynamically consistent. This interdependence of reactions and volume inevitably constrain their possible states and dynamics. In addition, the cycles themselves may not always proceed in the forward direction, which can result in shrinking, depending on the environmental conditions. It is nontrivial under what thermodynamic conditions a coherent forward cycle dynamics and volume growth can be achieved. Moreover, a steady cycling

and growth should accompany the thermodynamic cost. However, we lack a theoretical basis to address these fundamental problems of growing systems.

In this work, we establish the thermodynamics for growing systems. The difficulty in developing it lies in that the change in the volume affects all reactions in it. In the conventional theory of chemical reactions, reaction fluxes are described as functions of densities of chemicals (concentrations) [43–50], which presumes a constant volume. However, if the volume changes, the densities can change even though the numbers of chemicals remain unchanged. Hence, it is necessary to return to a thermodynamic formulation in which the numbers of chemicals and the volume are treated separately. In other words, we have to explicitly account of the extensivity of thermodynamic functions, which is scaled out when the densities alone are considered. Nevertheless, we should also retain the density representation and its dual representation by the chemical potentials to appropriately characterize steady growing states and the conditions imposed by the intensive variables of the environment.

We clarify this entangled relation among the triad of chemical numbers, densities and potentials by clarifying the geometric structure they form. This structure is built on the recently discovered Hessian geometric structure between chemical densities and potentials in a constant volume [51, 52] by additionally introducing the space of the numbers of chemicals. Based on the second law of thermodynamics, our theory classifies the thermodynamic conditions under which the system grows, shrinks or equilibrates. It also reveals the region in which the chemical density is constrained to a steady growth. Furthermore, it enables us to evaluate the entropy production rate, i.e., the physical cost of the steady growth. Our nonequilibrium system with volume growth has its origin in the extensivity of thermodynamics, which is different

from the conventional nonequilibrium systems with constant volume [43–50].

We emphasize that our derivation is performed based on a purely thermodynamic argument [51–54]. As a result, it does not depend on any particular form of thermodynamic potentials or reaction kinetics. Thus, our theory is widely applicable and contributes to understanding the origins of life and constructing protocells [13–24] as well as seeking the universal laws of biological cells [10–12, 32–38].

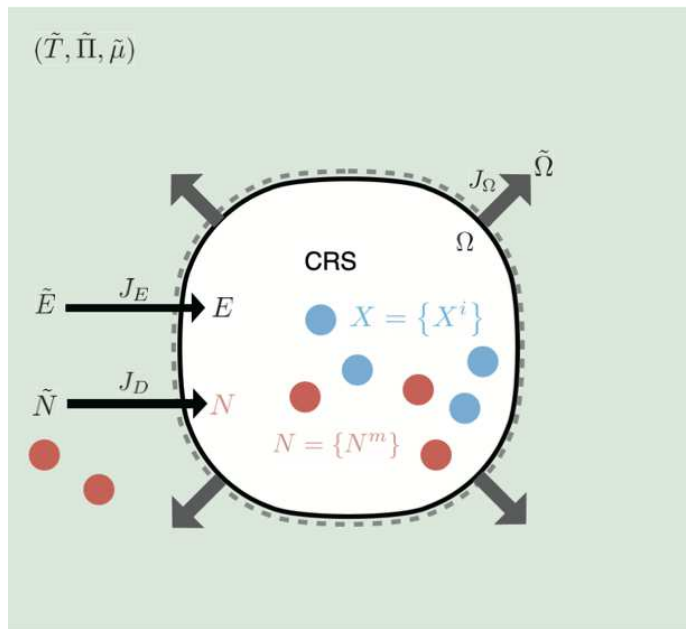
This paper is organized as follows. We devote Sec. II to outline our main results without showing the details of their derivation. From Sec. III onward, we start with the derivation of our main results. In Sec. III, we analyze the behavior of the total entropy function with respect to time for chemical reaction dynamics. We devote Sec. IV to the preparation for the geometric structure of growing systems. In Sec. V, we classify the environmental conditions to determine the fate of the system based on the form of the total entropy function. In Sec. VI, we consider the steady growing state and evaluate the entropy production rate in this state. We illustrate our theory in Sec. VII on the ideal gas as a specific example of thermodynamic potentials. In Sec. VIII, we numerically verify our theory by considering a specific example of a chemical reaction system composed of the ideal gas and obeying mass action kinetics. Finally, we summarize our work with further discussions in Sec. IX.

II. OUTLINE OF THE MAIN RESULTS

A. Thermodynamic setup

Let us start with the presentation of the setting of the system (FIG. 1). Consider a growing open chemical reaction system (CRS) surrounded by a reservoir. We assume that the system is always in a well-mixed state (a local equilibrium state), and therefore we can completely describe it by extensive variables (E, Ω, N, X) . Here, E and Ω represent the internal energy and the volume; $N = \{N^m\}$ denotes the number of chemicals that can move across the membrane between the system and the reservoir called open chemicals; meanwhile, $X = \{X^i\}$ is the number of chemicals confined within the system; the indices m and i respectively run from $m = 1$ to \mathcal{N}_N and from $i = 1$ to \mathcal{N}_X , where \mathcal{N}_N and \mathcal{N}_X are the numbers of species of the open and confined chemicals. The reservoir is characterized by intensive variables $(\tilde{T}, \tilde{\Pi}, \tilde{\mu})$, where \tilde{T} and $\tilde{\Pi}$ are the temperature and the pressure; $\tilde{\mu} = \{\tilde{\mu}_m\}$ is the chemical potential corresponding to the open chemicals. Also, we denote the corresponding extensive variables by $(\tilde{E}, \tilde{\Omega}, \tilde{N})$.

In thermodynamics, the entropy function is defined on (E, Ω, N, X) as a concave, smooth and homogeneous function $\Sigma[E, \Omega, N, X]$. We write the entropy function



Chemical Reaction System (CRS)

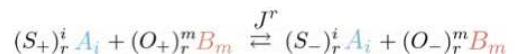


FIG. 1. Diagrammatic representation of open CRSs. The chemical reactions occur with the reaction fluxes $J(t) = \{J^r(t)\}$, the r th reaction of which is represented as the chemical equation at the bottom. Here, $A = \{A_i\}$ are the labels of the confined chemicals, and $B = \{B_m\}$ are the ones of the open chemicals which can move across the membrane with the diffusion fluxes $J_D(t) = \{J_D^m(t)\}$. The numbers of the confined and open chemicals in the system are denoted by $X = \{X^i\}$ and $N = \{N^m\}$, respectively. Also, $(S_+)_r^i$ and $(O_+)_r^m$ denote stoichiometric coefficients of the reactants in r th reaction, whereas $(S_-)_r^i$ and $(O_-)_r^m$ are the ones of the products. The stoichiometric matrices are given as $S_r^i = (S_-)_r^i - (S_+)_r^i$ and $O_r^m = (O_-)_r^m - (O_+)_r^m$. For theoretical simplicity, we ignore the tension of the membrane and assume that it never bursts.

for the reservoir as $\tilde{\Sigma}_{\tilde{T}, \tilde{\Pi}, \tilde{\mu}}[\tilde{E}, \tilde{\Omega}, \tilde{N}]$, and therefore the total entropy can be expressed as

$$\Sigma^{\text{tot}} = \Sigma[E, \Omega, N, X] + \tilde{\Sigma}_{\tilde{T}, \tilde{\Pi}, \tilde{\mu}}[\tilde{E}, \tilde{\Omega}, \tilde{N}], \quad (1)$$

where we use the additivity of the entropy. Furthermore, due to the homogeneity of the entropy function for the system, without loss of generality, we can write it as

$$\Sigma[E, \Omega, N, X] = \Omega \sigma[\epsilon, n, x], \quad (2)$$

where $\sigma[\epsilon, n, x]$ is the entropy density and $(\epsilon, n, x) := (E/\Omega, N/\Omega, X/\Omega)$. Since this work only treats a situation without phase transitions, we assume that $\sigma[\epsilon, n, x]$ is strictly concave.

Next, we define the dynamics for the system as

$$\begin{aligned} \frac{dE}{dt} &= J_E(t), \quad \frac{d\Omega}{dt} = J_\Omega(t), \\ \frac{dN^m}{dt} &= O_r^m J^r(t) + J_D^m(t), \quad \frac{dX^i}{dt} = S_r^i J^r(t), \end{aligned} \quad (3)$$

where $J_E(t)$, $J_\Omega(t)$, $J_D(t) = \{J_D^m(t)\}$ and $J(t) = \{J^r(t)\}$ represent the energy, the volume, the chemical diffusion and the chemical reaction fluxes, respectively; $S = \{S_r^i\}$ and $O = \{O_r^m\}$ denote stoichiometric matrices for the confined and the open chemicals (see FIG. 1). The index r runs from $r = 1$ to \mathcal{N}_R , where \mathcal{N}_R is the number of reactions. Also, in Eq. (3), we employed Einstein's summation convention for notational simplicity. The dynamics of the reservoir is given as

$$\frac{d\tilde{E}}{dt} = -J_E(t), \quad \frac{d\tilde{\Omega}}{dt} = -J_\Omega(t), \quad \frac{d\tilde{N}^m}{dt} = -J_D^m(t). \quad (4)$$

In this work, we assume that the time scale of the reactions is much slower than that of the others (that is, $J_E(t), J_\Omega(t), J_D(t) \gg J(t)$). Therefore, our dynamics is effectively governed only by the reaction flux $J(t)$ (see Sec. III for details). In addition, we consider minimal motifs of autocatalytic cycles, which were identified in [26] and characterized by the regularity of the stoichiometric matrix S for the confined chemicals, i.e., $\mathcal{N}_X = \mathcal{N}_R = \text{Rank}[S]$ (see Appendix A for details).

B. Thermodynamic potentials, duality, and total entropy characterizing the growing systems

With the above setup, we obtain a conjugate pair of thermodynamic potentials, $\varphi(x)$ and $\varphi^*(y)$, which play pivotal roles in our theory. The partial grand potential density $\varphi(x) = \varphi[\tilde{T}, \tilde{\mu}; x]$ is defined as

$$\varphi[\tilde{T}, \tilde{\mu}; x] := \min_{\epsilon, n} \left\{ \epsilon - \tilde{T}\sigma[\epsilon, n, x] - \tilde{\mu}_m n^m \right\}, \quad (5)$$

(see Sec. IV for details). The function $\varphi^*(y) = \varphi^*[\tilde{T}, \tilde{\mu}; y]$ is the full grand potential density obtained by the Legendre transformation of $\varphi(x)$ as

$$\varphi^*[\tilde{T}, \tilde{\mu}; y] := \max_x \{y_i x^i - \varphi(x)\}. \quad (6)$$

In conventional chemical thermodynamics with a constant volume, $\varphi(x)$ and $\varphi^*(y)$ characterize the system completely. They also work as the dual convex functions inducing the Hessian geometric structure of chemical thermodynamics [51, 52]. Because of the one-to-one correspondence of the Legendre transformation induced by $\varphi(x)$ and $\varphi^*(y)$, we can equivalently specify a state of the system either by the densities x or by its Legendre transform $y = \partial\varphi(x)$. The thermodynamic interpretation of y is the corresponding chemical potential to

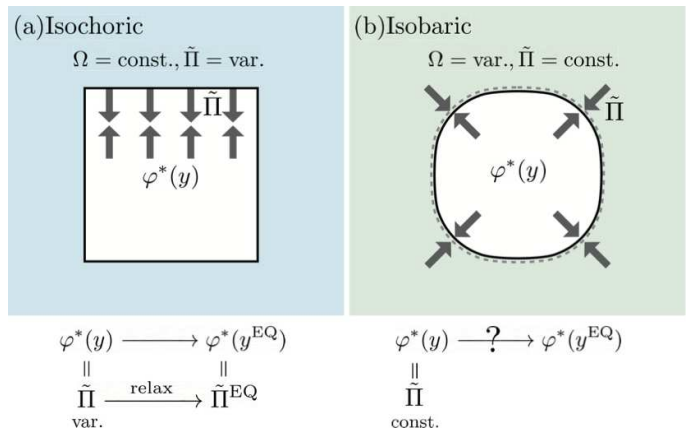


FIG. 2. Diagrammatic representation of (a) isochoric and (b) isobaric situations. (a) In the isochoric case, the external pressure $\tilde{\Pi}$ varies to keep the volume Ω constant. The internal pressure $\varphi^*(y)$, which always balances with $\tilde{\Pi}$, can converge to the chemical equilibrium pressure $\varphi^*(y^{\text{EQ}}) = \tilde{\Pi}^{\text{EQ}}$. (b) In the isobaric case, the volume Ω varies to keep the internal pressure $\varphi^*(y)$ always equal to the constant external pressure $\tilde{\Pi}$. Consequently, the internal pressure $\varphi^*(y) = \tilde{\Pi}$ may not balance with the chemical equilibrium pressure $\varphi^*(y^{\text{EQ}})$, which is specified by the chemical potentials $\tilde{\mu}$ in the reservoir. This imbalance drives growing or shrinking of the volume.

x . This dualistic representation is central to our theory. In addition, $\varphi^*(y)$ can be interpreted as the pressure of the system at the state y whose corresponding density is $x = \partial\varphi^*(y)$.

If the volume is fixed, the internal pressure $\varphi^*(y)$ always balances with the external pressure $\tilde{\Pi}$ incurred by the boundary to keep the volume $\tilde{\Omega}$ constant (see FIG. 2(a)). Furthermore, the internal pressure $\varphi^*(y) = \tilde{\Pi}$ converges to the pressure $\varphi^*(y^{\text{EQ}}) = \tilde{\Pi}^{\text{EQ}}$ at the chemical equilibrium state y^{EQ} . The state y^{EQ} is determined by the chemical potentials $\tilde{\mu}$ in the reservoir as

$$y_i^{\text{EQ}} = -\tilde{\mu}_m O_r^m (S^{-1})_i^r, \quad (7)$$

where S^{-1} is the inverse of the stoichiometric matrix S . In the density representation, the system converges to the chemical equilibrium state $x_{\text{EQ}} = \partial\varphi^*(y^{\text{EQ}})$.

By contrast, in growing systems under isobaric conditions, the volume can change. Due to the fast time scale of the volume flux $J_\Omega(t)$, the internal pressure $\varphi^*(y)$ is fixed by the external (reservoir) one $\tilde{\Pi}$ (see FIG. 2(b)). As a result, the volume at X is variationally determined as

$$\Omega(X) = \arg \min_{\Omega} \left\{ \Omega \varphi \left(\frac{X}{\Omega} \right) + \tilde{\Pi} \Omega \right\}. \quad (8)$$

Also, the chemical density x is a nonlinear function $\rho_X(X)$ of X as $x(X) = X/\Omega(X) =: \rho_X(X)$.

In this case, the internal pressure $\varphi^*(y)$ is restricted to the constant external pressure $\tilde{\Pi}$, whereas the chemical

equilibrium pressure $\varphi^*(y^{\text{EQ}})$ is specified by the chemical potentials $\tilde{\mu}$ in the reservoir. If $\varphi^*(y) = \tilde{\Pi}$ and $\varphi^*(y^{\text{EQ}})$ are not balanced, the system can not converge to the equilibrium state, and this imbalance drives growth or shrinking of the volume. Whether growth or shrinking occurs is determined by the second law and the functional form of total entropy, which is represented for growing systems as

$$\Sigma^{\text{tot}}(X) = \frac{\Omega(X)}{\tilde{T}} K^{\mathcal{Y}}(\rho^{\mathcal{Y}}(X)) + \text{const.}, \quad (9)$$

where $K^{\mathcal{Y}}(y)$ is defined as

$$K^{\mathcal{Y}}(y) := \varphi^*(y^{\text{EQ}}) - \tilde{\Pi} - \mathcal{D}^{\mathcal{Y}}[y^{\text{EQ}}||y]. \quad (10)$$

Here, $\mathcal{D}^{\mathcal{Y}}[y'||y]$ is the Bregman divergence [55–57] induced by $\varphi^*(y)$, and $y = \rho^{\mathcal{Y}}(X) = \partial\varphi(\rho_X(X))$ is a non-linear map to associate the number of chemicals X with a chemical potential y .

C. The conditions for growth, shirinking, and equilibration

Our first claim provides the condition that determines the fate of the system, i.e., growth, shirinking or equilibration.

Claim 1 *The fate of the system is classified by the sign of $\varphi^*(y^{\text{EQ}}) - \tilde{\Pi}$ as follows:*

1. *If and only if $\varphi^*(y^{\text{EQ}}) - \tilde{\Pi} = 0$, equilibrium states exist and the system converges to one of them.*
2. *If and only if $\varphi^*(y^{\text{EQ}}) - \tilde{\Pi} < 0$, the system eventually shrinks and finally vanishes.*
3. *If and only if $\varphi^*(y^{\text{EQ}}) - \tilde{\Pi} > 0$, the system is growing.*

(see Sec. V and Theorem 1 for details).

This result indicates that the system equilibrates only if the pressure $\tilde{\Pi}$ specified by the reservoir happens to coincide with the chemical equilibrium pressure $\varphi^*(y^{\text{EQ}})$ specified by the reservoir chemical potentials $\tilde{\mu}$. Otherwise, the system shrinks or grows.

Example 1: To give an intuitive illustration, we consider a minimal motif of autocatalytic cycles (see FIG. 3(a)). Here, two confined chemicals $A = (A_1, A_2)$ and two open chemicals $B = (B_1, B_2)$ are involved in the two reactions R_1 and R_2 . We can regard the open chemicals B_1 and B_2 as a resource and waste, respectively, because they are consumed and produced when the forward reactions progress. The stoichiometric matrices can

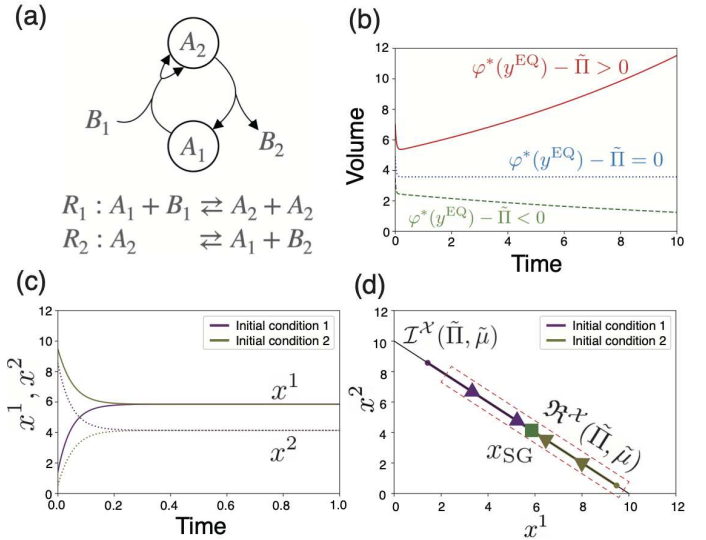


FIG. 3. (a) A graph representation and chemical equations of a minimal motif of autocatalytic cycles. Two confined chemicals $A = (A_1, A_2)$ and two open chemicals $B = (B_1, B_2)$ undergo the two reactions R_1 and R_2 . (b) The time evolution of the volume of the system for different parameter sets (see the caption in FIG. 8 for specific values of the parameters). The fate of the system is classified by the sign of $\varphi^*(y^{\text{EQ}}) - \tilde{\Pi}$. (c) The time evolution of the densities (x^1, x^2) of the confined chemicals (A_1, A_2) for the growth case $\varphi^*(y^{\text{EQ}}) - \tilde{\Pi} > 0$. The evolutions are shown for two different initial conditions 1 and 2. (d) The trajectories of the system in the density space. They are constrained to the isobaric manifold $\mathcal{I}^{\mathcal{X}}(\tilde{\Pi}, \tilde{\mu})$. In this example, the system converges to a steady growing state x_{SG} (green square), irrespective of the initial conditions. Such a steady growing state must be in the region $\mathfrak{R}^{\mathcal{X}}(\tilde{\Pi}, \tilde{\mu}) \subset \mathcal{I}^{\mathcal{X}}(\tilde{\Pi}, \tilde{\mu})$, highlighted by the red dashed rectangle.

be represented as

$$S = \begin{matrix} & R_1 & R_2 \\ \begin{matrix} A_1 \\ A_2 \end{matrix} & \begin{pmatrix} -1 & 1 \\ 2 & -1 \end{pmatrix}, & O = \begin{matrix} B_1 & B_2 \\ \begin{pmatrix} -1 & 0 \\ 0 & 1 \end{pmatrix}. \end{matrix} \quad (11)$$

The regularity of the matrix S is confirmed by $\det[S] = -1 \neq 0$. Denoting the number of $A = (A_1, A_2)$ by $X = (X^1, X^2)$, the reaction dynamics for the confined chemicals is written as

$$\frac{dX^i}{dt} = S_r^i J^r(t). \quad (12)$$

In this example, we employ mass action kinetics with the local detailed balance condition [43, 44, 51, 52, 58] for the reaction flux $J(t)$ (see Sec. VIII for details). Furthermore, we assume the ideal gas potential: the functional form of $\varphi^*(y)$ is obtained as

$$\varphi^*(y) = R\tilde{T} \left[\sum_i e^{\frac{y_i - \nu_i^o(\tilde{T})}{R\tilde{T}}} + \sum_m e^{\frac{\tilde{\mu}_m - \mu_m^o(\tilde{T})}{R\tilde{T}}} \right],$$

(see Eq. (59) in Sec. VII for a derivation). The volume $\Omega(t)$ can be calculated by the equation of state,

$$\Omega(X) = \frac{RT \sum_i X^i}{\tilde{\Pi} - RT \sum_m \tilde{n}^m}, \quad (13)$$

(see Eq. (67) in Sec. VII for details). In FIG. 3(b), we verified Claim 1 by numerical simulation. Indeed, the fate of the system is classified by the sign of $\varphi^*(y^{\text{EQ}}) - \tilde{\Pi}$. \square

D. Thermodynamic constraint of isobaric dynamics

Under isobaric conditions with a fast volume flux $J_\Omega(t)$, the pressure of the system should balance with the pressure of the reservoir. This constraint naturally defines the isobaric manifold in the chemical potential space:

$$\mathcal{I}^\mathcal{V}(\tilde{\Pi}, \tilde{\mu}) := \{y | \varphi^*(y) - \tilde{\Pi} = 0\}. \quad (14)$$

Its Legendre transform $\mathcal{I}^\mathcal{X}(\tilde{\Pi}, \tilde{\mu}) := \partial\varphi^*(\mathcal{I}^\mathcal{V})$ is a hypersurface in the density space. Thus, $\mathcal{I}^\mathcal{X}(\tilde{\Pi}, \tilde{\mu})$ and $\mathcal{I}^\mathcal{V}(\tilde{\Pi}, \tilde{\mu})$ characterize the thermodynamically admissible submanifolds in the density and chemical potential spaces, respectively.

Example 2: For the autocatalytic motif in FIG. 3(a), the time evolution of $x(t)$ is shown in FIG. 3(c) for the growth case in FIG. 3(b). This time evolution is actually constrained to the isobaric manifold $\mathcal{I}^\mathcal{X}(\tilde{\Pi}, \tilde{\mu})$ as shown in FIG. 3(d). Since we have assumed ideal gas potentials, the isobaric manifold $\mathcal{I}^\mathcal{X}(\tilde{\Pi}, \tilde{\mu})$ reduces to a simplex by the equation of state (see Sec. VII for details). \square

E. The constraints and thermodynamic properties associated with the steady growing state

Finally, we clarify the additional constraint imposed on the steady growing state x_{SG} . The steady growing state is defined as a state such that the density remains constant with time whereas the volume keeps increasing [39–42]. For the autocatalytic motif shown in FIG. 3(a), such a state x_{SG} exists and $x(t)$ converges to a steady growing state as in FIG. 3(c, d).

At this state, the entropy production rate can be expressed as

$$\dot{\Sigma}^{\text{tot}}(\Omega(t) x_{\text{SG}}) = \frac{\dot{\Omega}(t)}{\tilde{T}} K^\mathcal{V}(y^{\text{SG}}), \quad (15)$$

where y^{SG} the Legendre transform of x_{SG} by $\partial\varphi$. Because $\dot{\Omega}(t) > 0$ at the growing state, $K^\mathcal{V}(y^{\text{SG}})$ should be positive by the second law. This requirement implies that y^{SG}

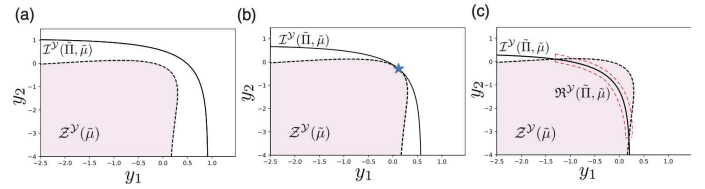


FIG. 4. Transition from the shrinking to the growing case. The isobaric manifold $\mathcal{I}^\mathcal{V}(\tilde{\Pi}, \tilde{\mu})$ and the region $\mathcal{Z}^\mathcal{V}(\tilde{\mu})$ in the chemical potential space are indicated by the solid curve and the light purple color, respectively. (a) When $\varphi^*(y^{\text{EQ}}) - \tilde{\Pi} < 0$ holds (i.e., the shrinking case), the intersection does not exist. (b) When $\varphi^*(y^{\text{EQ}}) - \tilde{\Pi} = 0$ holds (i.e., the equilibrating case), transition from shrinking to growing occurs. (c) When $\varphi^*(y^{\text{EQ}}) - \tilde{\Pi} > 0$ holds (i.e., the growing case), the intersection $\mathfrak{R}^\mathcal{V}(\tilde{\Pi}, \tilde{\mu}) = \mathcal{I}^\mathcal{V}(\tilde{\Pi}, \tilde{\mu}) \cap \mathcal{Z}^\mathcal{V}(\tilde{\mu})$ exists, which is highlighted by the curved red rectangle.

should lie in the region $\mathfrak{R}^\mathcal{V}(\tilde{\Pi}, \tilde{\mu}) = \mathcal{I}^\mathcal{V}(\tilde{\Pi}, \tilde{\mu}) \cap \mathcal{Z}^\mathcal{V}(\tilde{\mu})$. Here,

$$\mathcal{Z}^\mathcal{V}(\tilde{\mu}) := \{y | \varphi^*(y^{\text{EQ}}) - \varphi^*(y) - \mathcal{D}^\mathcal{V}[y^{\text{EQ}} || y] > 0\}, \quad (16)$$

designates the region in which the positivity of entropy production is guaranteed. By transferring this condition into the density space by the Legendre transformation, we have the following claim for x_{SG} :

Claim 2 *When $\varphi^*(y^{\text{EQ}}) - \tilde{\Pi} > 0$ and a steady growing state x_{SG} exists, the state x_{SG} must be in the region $\mathfrak{R}^\mathcal{X}(\tilde{\Pi}, \tilde{\mu})$, where $\mathfrak{R}^\mathcal{X}(\tilde{\Pi}, \tilde{\mu}) = \partial\varphi^*(\mathfrak{R}^\mathcal{V})$. The entropy production rate at the state x_{SG} is represented as Eq. (15). (See Sec. VI and Theorem 2 for the details)*

Example 3: For the autocatalytic motif in FIG. 3(a), the steady growing state x_{SG} is indeed located within the region $\mathfrak{R}^\mathcal{X}(\tilde{\Pi}, \tilde{\mu})$ (see FIG. 3(d)).

Moreover, we can verify that the transition from the shrinking to the growing case occurs when the intersection between $\mathcal{I}^\mathcal{V}(\tilde{\Pi}, \tilde{\mu})$ and $\mathcal{Z}^\mathcal{V}(\tilde{\mu})$ appears (see FIG. 4(b)). In FIG. 4, the isobaric manifold $\mathcal{I}^\mathcal{V}(\tilde{\Pi}, \tilde{\mu})$ and the region $\mathcal{Z}^\mathcal{V}(\tilde{\mu})$ are indicated in the chemical potential space. For the shrinking case (FIG. 4(a)), the intersection is empty. By contrast, for the growing case (FIG. 4(c)), the intersection exists. \square

This concludes the outline of all our main results, which consist of the condition of growth, the constraints of growing systems and steady growing states, and the forms of total entropy and entropy production at the steady growing state.

III. THERMODYNAMICS FOR GROWING SYSTEMS

From this section onward, we work on the derivation of our main claims introduced in Sec. II. In this section, we derive the form of the total entropy, Eq. (1), more specifically by employing time-scale separation. As a result, we will obtain the total entropy function for the reaction dynamics, Eq. (23). Also, we will show that, given the number of the confined chemicals X , the volume Ω of the system is determined by the variational form, Eq. (19), with the partial grand potential, Eq. (18).

Since we have assumed that $J_E(t), J_\Omega(t), J_D(t) \gg J(t)$, we can analyze the dynamics, Eqs. (3) and (4), by separating the fast ones $J_E(t), J_\Omega(t), J_D(t)$ and the slow one $J(t)$. By solving the fast dynamics using the second law (see Appendix B), we obtain the effective slow dynamics (the reaction dynamics) as

$$\begin{aligned} \frac{dX^i}{dt} &= S_r^i J^r(t), \quad \frac{d\tilde{E}}{dt} = -\frac{dE_{\text{QEQ}}(X)}{dt}, \\ \frac{d\tilde{\Omega}}{dt} &= -\frac{d\Omega_{\text{QEQ}}(X)}{dt}, \quad \frac{d\tilde{N}^m}{dt} = O_r^m J^r(t) - \frac{dN_{\text{QEQ}}^m(X)}{dt}, \end{aligned} \quad (17)$$

where $(\cdot)_{\text{QEQ}}$ represents the value at the equilibrium state of the fast dynamics. We call this the quasi-equilibrium state, because it is not the equilibrium state of the slow dynamics. By using the partial grand potential:

$$\Phi[\tilde{T}, \tilde{\mu}; \Omega, X] := \min_{E, N} \left\{ E - \tilde{T}\Sigma[E, \Omega, N, X] - \tilde{\mu}_m N^m \right\}, \quad (18)$$

the volume at the quasi-equilibrium state with the number of the confined chemicals X can be evaluated by the variational form:

$$\Omega_{\text{QEQ}}(X) = \arg \min_{\Omega} \left\{ \Phi[\tilde{T}, \tilde{\mu}; \Omega, X] + \tilde{\Pi}\Omega \right\}. \quad (19)$$

In addition, the other extensive variables can be calculated by differentiations of $\Phi[\tilde{T}, \tilde{\mu}; \Omega_{\text{QEQ}}, X]$ as

$$\begin{aligned} \Sigma_{\text{QEQ}}(X) &= -\frac{\partial \Phi[\tilde{T}, \tilde{\mu}; \Omega_{\text{QEQ}}, X]}{\partial \tilde{T}}, \\ N_{\text{QEQ}}^m(X) &= -\frac{\partial \Phi[\tilde{T}, \tilde{\mu}; \Omega_{\text{QEQ}}, X]}{\partial \tilde{\mu}_m}, \\ E_{\text{QEQ}}(X) &= \Phi[\tilde{T}, \tilde{\mu}; \Omega_{\text{QEQ}}, X] - \tilde{T} \frac{\partial \Phi[\tilde{T}, \tilde{\mu}; \Omega_{\text{QEQ}}, X]}{\partial \tilde{T}} \\ &\quad - \tilde{\mu}_m \frac{\partial \Phi[\tilde{T}, \tilde{\mu}; \Omega_{\text{QEQ}}, X]}{\partial \tilde{\mu}_m}, \end{aligned} \quad (20)$$

where $\Sigma_{\text{QEQ}}(X)$ is the abbreviation of $\Sigma[E_{\text{QEQ}}, \Omega_{\text{QEQ}}, N_{\text{QEQ}}, X]$. The details of the derivation are shown in Appendix B. The formal solution of Eq.

(17) with the initial condition $(X_0, \tilde{E}(0), \tilde{\Omega}(0), \tilde{N}(0))$ is represented as

$$\begin{aligned} X^i(t) &= X_0^i + S_r^i \Xi^r(t), \\ \tilde{E}(t) &= \tilde{E}(0) - E_{\text{QEQ}}(X(t)), \\ \tilde{\Omega}(t) &= \tilde{\Omega}(0) - \Omega_{\text{QEQ}}(X(t)), \\ \tilde{N}^m(t) &= \tilde{N}^m(0) + O_r^m \Xi^r(t) - N_{\text{QEQ}}^m(X(t)), \end{aligned} \quad (21)$$

where $\Xi(t) = \{\Xi^r(t)\}$ is the integration of $J(t)$ with the initial condition $\Xi(0) = 0$; this is known as the extent of reaction in chemistry. Since we have assumed that S is regular, there are no stoichiometric constraints that restrict attainable state of $X(t)$ by its initial state $X(0)$; i.e., the stoichiometric compatibility class [50–52] becomes $\mathbb{R}_{>0}^{N_X}$. Furthermore, by using the inverse matrix S^{-1} , the last equation in Eq. (21) can be rewritten as

$$\tilde{N}^m(t) = O_r^m (S^{-1})_i^r X^i(t) - N_{\text{QEQ}}^m(X(t)) + \text{const.}, \quad (22)$$

where we substitute $\Xi^r(t) = (S^{-1})_i^r \{X^i(t) - X_0^i\}$ into the last equation and abbreviate the terms composed of the initial condition to “const.”. The representation of Eq. (22) implies that our reaction dynamics can be completely described only by the time evolution of the confined chemicals, $X(t)$.

Next, we consider the time evolution of the total entropy during the reaction dynamics. By substituting Eqs. (21) and (22) into Eq. (1), we obtain

$$\begin{aligned} \Sigma^{\text{tot}}(X) &= \Sigma_{\text{QEQ}}(X) - \frac{1}{\tilde{T}} E_{\text{QEQ}}(X) - \frac{\tilde{\Pi}}{\tilde{T}} \Omega_{\text{QEQ}}(X) \\ &\quad + \frac{\tilde{\mu}_m}{\tilde{T}} N_{\text{QEQ}}^m(X) - \frac{\tilde{\mu}_m}{\tilde{T}} O_r^m (S^{-1})_i^r X^i + \text{const.} \\ &= -\frac{1}{\tilde{T}} \left\{ \Phi[\tilde{T}, \tilde{\mu}; \Omega_{\text{QEQ}}, X] + \tilde{\Pi}\Omega_{\text{QEQ}}(X) - y_i^{\text{EQ}} X^i \right\} \\ &\quad + \text{const.}, \end{aligned} \quad (23)$$

where we employ the Taylor expansion for $\tilde{\Sigma}_{\tilde{T}, \tilde{\Pi}, \tilde{\mu}}$ and the partial grand potential, Eq. (18); for simplicity, we also define

$$y_i^{\text{EQ}} := -\tilde{\mu}_m O_r^m (S^{-1})_i^r. \quad (24)$$

According to the second law, the system must climb up the landscape determined by the concave function $\Sigma^{\text{tot}}(X)$ and finally converge to its maximum, which is called the equilibrium state [59], if it exists. Therefore, to elucidate the fate of the system, it is important to analyze the form of the concave function $\Sigma^{\text{tot}}(X)$. We can briefly classify the form of $\Sigma^{\text{tot}}(X)$ into the following three cases: (1) If $\Sigma^{\text{tot}}(X)$ is bounded above and the points attaining its maximum are in the interior of the domain of X , that is $\arg \max_X \{\Sigma^{\text{tot}}(X)\} \in \mathbb{R}_{>0}^{N_X}$, equilibrium states exist and the system converges to one of them. (2) If $\Sigma^{\text{tot}}(X)$ is bounded above and the maximum of $\Sigma^{\text{tot}}(X)$ is at $X = 0$, the volume $\Omega_{\text{QEQ}}(X(t))$ eventually shrinks and finally vanishes. (3) If $\Sigma^{\text{tot}}(X)$

is not bounded above, $X(t)$ diverges in the reaction dynamics. Also, the volume $\Omega_{\text{QEQ}}(X)$ diverges for $X \rightarrow \infty$, because of the homogeneity of the volume. This situation corresponds to the growth of the system. The main aim of this work is to reveal what condition distinguishes these three cases. In the remaining part of this paper, we will address this problem by employing Hessian and projective geometry.

IV. PREPARATION FOR A GEOMETRIC REPRESENTATION OF ISOBARIC CHEMICAL REACTION SYSTEMS

We devote this section to preparation for the geometric representation of our system. As mentioned in Sec. II, the homogeneity of the system entropy function allows us to write it as

$$\Sigma[E, \Omega, N, X] = \Omega \sigma[\epsilon, n, x], \quad (25)$$

where $\sigma[\epsilon, n, x]$ represents the entropy density and $(\epsilon, n, x) := (E/\Omega, N/\Omega, X/\Omega)$; also, we have assumed that $\sigma[\epsilon, n, x]$ is strictly concave. We introduce the number and the density spaces of the confined chemicals as $X \in \mathfrak{X} = \mathbb{R}_{>0}^{N_X}$ and $x \in \mathcal{X} = \mathbb{R}_{>0}^{N_X}$, respectively. Also, we define the partial grand potential density as $\varphi(x) = \varphi[\tilde{T}, \tilde{\mu}; x] := \Omega^{-1} \Phi[\tilde{T}, \tilde{\mu}; \Omega, X] = \Phi[\tilde{T}, \tilde{\mu}; 1, X/\Omega]$, where we use the homogeneity of Φ . From the definition of Φ , Eq. (18), $\varphi[\tilde{T}, \tilde{\mu}; x]$ can be represented by a variant of the Legendre transformation of $\sigma[\epsilon, n, x]$ as

$$\varphi[\tilde{T}, \tilde{\mu}; x] = \min_{\epsilon, n} \left\{ \epsilon - \tilde{T} \sigma[\epsilon, n, x] - \tilde{\mu}_m n^m \right\}, \quad (26)$$

and therefore $\varphi(x)$ is strictly convex. By using $\varphi(x)$, we can rewrite Eq. (19) as

$$\Omega(X) = \Omega_{\text{QEQ}}(X) = \arg \min_{\Omega} \left\{ \Omega \varphi \left(\frac{X}{\Omega} \right) + \tilde{\Pi} \Omega \right\}. \quad (27)$$

For notational simplicity, we omit the subscript $(\cdot)_{\text{QEQ}}$ hereafter. Due to the strict convexity of $\varphi(x)$, the volume $\Omega(X)$ uniquely exists for any given X (see Appendix C).

Next, we define a map from the number space \mathfrak{X} to the density space \mathcal{X} :

$$\rho_{\mathcal{X}} : X \in \mathfrak{X} \mapsto \rho_{\mathcal{X}}(X) = \left\{ \rho_{\mathcal{X}}^i(X) \right\} = \frac{X^i}{\Omega(X)} \in \mathcal{X}, \quad (28)$$

which gives the densities of the confined chemicals at the quasi-equilibrium state with X . Because of homogeneity, $\Omega(\alpha X) = \alpha \Omega(X)$ ($\alpha > 0$), which is guaranteed by Eq. (27), the map $\rho_{\mathcal{X}}$ satisfies

$$\rho_{\mathcal{X}}(\alpha X) = \rho_{\mathcal{X}}(X). \quad (29)$$

To clarify the geometric interpretation of the map $\rho_{\mathcal{X}}$, we regard the number space \mathfrak{X} as a collection of rays; that

is, we define the projective space of \mathfrak{X} as $\mathcal{P}\mathfrak{X}$. Elements of $\mathcal{P}\mathfrak{X}$ are subsets $\mathfrak{r} \subset \mathfrak{X}$ such that any two points X and X' are in the same subset (i.e., on the ray \mathfrak{r} [60]) if and only if $X = \alpha X'$ ($\alpha > 0$) (see FIG. 5(a)). Due to Eq. (29), the map $\rho_{\mathcal{X}}$ descends to a well-defined map from $\mathcal{P}\mathfrak{X}$ to \mathcal{X} :

$$\bar{\rho}_{\mathcal{X}} : \mathfrak{r} \in \mathcal{P}\mathfrak{X} \mapsto \bar{\rho}_{\mathcal{X}}(\mathfrak{r}) = \rho_{\mathcal{X}}(X) \in \mathcal{X}, \text{ for } X \in \mathfrak{r}. \quad (30)$$

Also, Eq. (28) implies that the above map is injective [61]. The range of the map $\bar{\rho}_{\mathcal{X}}$, denoted by $\text{Ran}[\bar{\rho}_{\mathcal{X}}]$, is calculated by solving the variational form, Eq. (27), as follows. The critical equation of Eq. (27) is given as

$$\varphi \left(\frac{X}{\Omega} \right) - \frac{X^i}{\Omega} \partial_i \varphi \left(\frac{X}{\Omega} \right) + \tilde{\Pi} = 0, \quad (31)$$

where $\partial_i \varphi(X/\Omega) = \partial \varphi(x) / \partial x^i|_{x=X/\Omega}$. Therefore, by defining the isobaric manifold:

$$\mathcal{I}^{\mathcal{X}}(\tilde{\Pi}, \tilde{\mu}) := \left\{ x | \varphi(x) - x^i \partial_i \varphi(x) + \tilde{\Pi} = 0 \right\}, \quad (32)$$

we obtain $\text{Ran}[\bar{\rho}_{\mathcal{X}}] = \mathcal{I}^{\mathcal{X}}(\tilde{\Pi}, \tilde{\mu})$. In other words, the time evolution of the density $x(t)$, given by Eq. (17), is constrained within this submanifold in \mathcal{X} . If we restrict the codomain of $\bar{\rho}_{\mathcal{X}}$ to $\mathcal{I}^{\mathcal{X}}(\tilde{\Pi}, \tilde{\mu})$, the map $\bar{\rho}_{\mathcal{X}} : \mathcal{P}\mathfrak{X} \rightarrow \mathcal{I}^{\mathcal{X}}(\tilde{\Pi}, \tilde{\mu})$ is bijective. For a later analysis, we also define the inverse map of $\bar{\rho}_{\mathcal{X}}$ as $\bar{\rho}_{\mathcal{X}}^{-1} : \mathcal{I}^{\mathcal{X}}(\tilde{\Pi}, \tilde{\mu}) \rightarrow \mathcal{P}\mathfrak{X}$, which gives the corresponding ray to a given density $x \in \mathcal{I}^{\mathcal{X}}(\tilde{\Pi}, \tilde{\mu})$ (see FIG. 5(a)).

Finally, we introduce the dual space of the density space \mathcal{X} as $\mathcal{Y} = \mathbb{R}^{N_X}$, which has the thermodynamic interpretation as the space of chemical potentials. Also, we define a map from \mathcal{X} to \mathcal{Y} by using the convex function $\varphi(x)$ as

$$\partial \varphi : x \in \mathcal{X} \mapsto \partial \varphi(x) = \left\{ \partial_i \varphi \right\} = \left\{ \frac{\partial \varphi}{\partial x^i} \right\} \in \mathcal{Y}, \quad (33)$$

which yields the values of the chemical potentials at a state x . Since $\varphi(x)$ is strictly convex, the map $\partial \varphi$ is injective. Furthermore, for ordinary chemical reaction systems, $\text{Ran}[\partial \varphi]$ is \mathbb{R}^{N_X} ; thus $\partial \varphi$ is bijective. To construct the inverse map of $\partial \varphi$, we define the strictly convex function $\varphi^*(y)$ on the dual space \mathcal{Y} by the Legendre transformation:

$$\varphi^*(y) := \max_x \left\{ y_i x^i - \varphi(x) \right\}, \quad (34)$$

which corresponds to the full grand potential density and gives the pressure of the system at a state y . Employing $\varphi^*(y)$, we can represent the inverse map as

$$\partial \varphi^* : y \in \mathcal{Y} \mapsto \partial \varphi^*(y) = \left\{ \partial^i \varphi^* \right\} = \left\{ \frac{\partial \varphi^*}{\partial y^i} \right\} \in \mathcal{X}. \quad (35)$$

These two spaces, \mathcal{X} and \mathcal{Y} , together with the pair of convex functions, $\varphi(x)$ and $\varphi^*(y)$, constitute the Hessian

geometric structure of chemical thermodynamics. The structure is fundamental to capture the geometric relation between the two dual spaces and is used intensively in the subsequent derivation.

The isobaric manifold $\mathcal{I}^{\mathcal{X}}(\tilde{\Pi}, \tilde{\mu})$ in \mathcal{X} is mapped via $\partial\varphi$ to the chemical potential space \mathcal{Y} as

$$\mathcal{I}^{\mathcal{Y}}(\tilde{\Pi}, \tilde{\mu}) := \partial\varphi(\mathcal{I}^{\mathcal{X}}) = \{y | \varphi^*(y) - \tilde{\Pi} = 0\}, \quad (36)$$

which is a level hypersurface for the dual convex function $\varphi^*(y)$ (see FIG. 5(a)). In addition, we define the map from \mathcal{X} to $\mathcal{I}^{\mathcal{Y}}(\tilde{\Pi}, \tilde{\mu}) \subset \mathcal{Y}$ as $\rho^{\mathcal{Y}} := \partial\varphi \circ \rho_{\mathcal{X}}$, which also induces the map:

$$\bar{\rho}^{\mathcal{Y}} : \tau \in \mathcal{P}\mathcal{X} \mapsto \bar{\rho}^{\mathcal{Y}}(\tau) = \rho^{\mathcal{Y}}(X) \in \mathcal{I}^{\mathcal{Y}}, \text{ for } X \in \tau. \quad (37)$$

Since this map is bijective, we define inverse map as $(\bar{\rho}^{\mathcal{Y}})^{-1} = \bar{\rho}_{\mathcal{X}}^{-1} \circ \partial\varphi^*$ (see FIG. 5(b)). The fact that the isobaric manifold is identical to a level hypersurface for a potential function is one of the fundamental constituents in the Hessian geometry.

V. FORM OF THE TOTAL ENTROPY FUNCTION AND THE FATE OF THE SYSTEM

With the preparation in the previous section, we are in the position to reveal the form of the total entropy function, Eq. (23), and predict the fate of the system.

For this purpose, we introduce the Bregman divergence [55–57] on \mathcal{Y} :

$$\mathcal{D}^{\mathcal{Y}}[y||y'] := \{\varphi^*(y) - \varphi^*(y')\} - \partial^i \varphi^*(y') \{y_i - y'_i\}, \quad (38)$$

which measures the deviation at the point y between the convex function $\varphi^*(y)$ and the tangent plane at the point y' . This divergence has the following property: $\mathcal{D}^{\mathcal{Y}}[y||y'] \geq 0$, the equality holds if and only if $y = y'$ and therefore it acts as an asymmetric distance from y' to y . The Bregman divergence is also one of the fundamental constituents of Hessian geometry.

We rewrite the total entropy function Eq. (23) by using the divergence as follows. Using the partial grand potential density $\varphi(x)$, Eq. (23) can be represented as

$$\Sigma^{\text{tot}}(X) = -\frac{\Omega(X)}{\tilde{T}} \left\{ \varphi(\rho_{\mathcal{X}}(X)) - y_i^{\text{EQ}} \rho_{\mathcal{X}}^i(X) + \tilde{\Pi} \right\}, \quad (39)$$

where the map $\rho_{\mathcal{X}}$ is defined in Eq. (28) and we neglect the constant term. This equation is further rearranged as

$$\begin{aligned} \Sigma^{\text{tot}}(X) &= \frac{\Omega(X)}{\tilde{T}} \left\{ y_i^{\text{EQ}} - \partial_i \varphi(\rho_{\mathcal{X}}(X)) \right\} \rho_{\mathcal{X}}^i(X) \\ &= \frac{\Omega(X)}{\tilde{T}} \left\{ y_i^{\text{EQ}} - \rho_i^{\mathcal{Y}}(X) \right\} \partial^i \varphi^*(\rho^{\mathcal{Y}}(X)), \end{aligned} \quad (40)$$

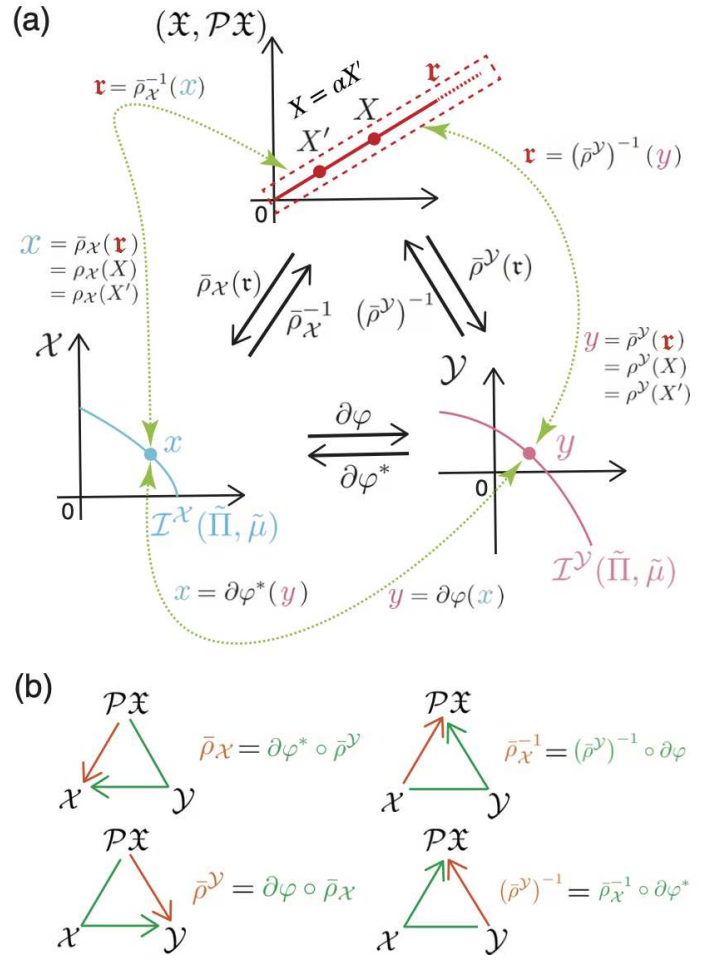


FIG. 5. Diagrammatic representation of the triad of spaces, $(\mathfrak{X}, \mathcal{P}\mathfrak{X})$, \mathcal{X} , and \mathcal{Y} . (a) The top space, $\mathfrak{X} = \mathbb{R}_{>0}^{\mathcal{N}_{\mathcal{X}}}$, represents the number of the confined chemicals X . We also define the set of rays in \mathfrak{X} as $\mathcal{P}\mathfrak{X}$. An element $\tau \in \mathcal{P}\mathfrak{X}$ is a subset of \mathfrak{X} such that any two points X and X' on the ray τ satisfy $X = \alpha X'$ ($\alpha > 0$). The spaces on the bottom left and bottom right represent the density space $\mathcal{X} = \mathbb{R}_{>0}^{\mathcal{N}_{\mathcal{X}}}$ and the chemical potential space $\mathcal{Y} = \mathbb{R}^{\mathcal{N}_{\mathcal{X}}}$, respectively. A ray $\tau \in \mathcal{P}\mathfrak{X}$ and a point x in the isobaric manifold $\mathcal{I}^{\mathcal{X}}(\tilde{\Pi}, \tilde{\mu}) \subset \mathcal{X}$ are mapped to each other by $\bar{\rho}_{\mathcal{X}}(\tau)$ and $\bar{\rho}_{\mathcal{X}}^{-1}(x)$. Similarly, a ray τ and a point y in the isobaric manifold $\mathcal{I}^{\mathcal{Y}}(\tilde{\Pi}, \tilde{\mu}) \subset \mathcal{Y}$ are mapped to each other by $\bar{\rho}^{\mathcal{Y}}(\tau)$ and $(\bar{\rho}^{\mathcal{Y}})^{-1}(y)$. The spaces, \mathcal{X} and \mathcal{Y} , are mapped to each other by $\partial\varphi$ and $\partial\varphi^*$. (b) The map $\bar{\rho}_{\mathcal{X}}$ from $\mathcal{P}\mathfrak{X}$ to \mathcal{X} and its inverse $\bar{\rho}_{\mathcal{X}}^{-1}$ can be represented by the composition of two maps via the space \mathcal{Y} (top line). Similarly, the map $\bar{\rho}^{\mathcal{Y}}$ from $\mathcal{P}\mathfrak{X}$ to \mathcal{Y} and its inverse $(\bar{\rho}^{\mathcal{Y}})^{-1}$ are expressed by the composition of two maps via the space \mathcal{X} (bottom line).

where we use Eq. (32) in the first line and $\rho_{\mathcal{X}} = \partial\varphi^* \circ \partial\varphi \circ \rho_{\mathcal{X}} = \partial\varphi^* \circ \rho^{\mathcal{Y}}$ in the second line. Finally, using the Bregman divergence from $\rho^{\mathcal{Y}}(X)$ to y^{EQ} , we obtain

$$\Sigma^{\text{tot}}(X) = \frac{\Omega(X)}{\tilde{T}} \left\{ \varphi^*(y^{\text{EQ}}) - \tilde{\Pi} - \mathcal{D}^{\mathcal{Y}}[y^{\text{EQ}}||\rho^{\mathcal{Y}}(X)] \right\}, \quad (41)$$

where we employ $\varphi^*(\rho^{\mathcal{Y}}(X)) = \tilde{\Pi}$, because $\rho^{\mathcal{Y}}(X) \in \mathcal{I}^{\mathcal{Y}}(\tilde{\Pi}, \tilde{\mu})$ (see Eq. (36)). Here, we note that the first two terms in Eq. (41), $\varphi^*(y^{\text{EQ}}) - \tilde{\Pi}$, are calculated by the intensive variables of the reservoir, because y^{EQ} is given by its chemical potential $\tilde{\mu}$ as in Eq. (24). In the following, we will show that the sign of $\varphi^*(y^{\text{EQ}}) - \tilde{\Pi}$ determines the fate of the system. For convenience, we also denote terms in the bracket in Eq. (41) by

$$K^{\mathcal{Y}}(y) := \varphi^*(y^{\text{EQ}}) - \tilde{\Pi} - \mathcal{D}^{\mathcal{Y}}[y^{\text{EQ}}|y], \quad (42)$$

that is, $\Sigma^{\text{tot}}(X) = \{\Omega(X)/\tilde{T}\}K^{\mathcal{Y}}(\rho^{\mathcal{Y}}(X))$.

First, let us consider the case $\varphi^*(y^{\text{EQ}}) - \tilde{\Pi} = 0$, which corresponds to the situation that equilibrium states exist and the system converges to one of them. In this case, since $K^{\mathcal{Y}}(y) = -\mathcal{D}^{\mathcal{Y}}[y^{\text{EQ}}|y]$ and $\Omega(X) > 0$, the entropy function in Eq. (41) satisfies $\Sigma^{\text{tot}}(X) \leq 0$, the equality holds if and only if $y = y^{\text{EQ}}$. Furthermore, from Eq. (36), $y^{\text{EQ}} \in \mathcal{I}^{\mathcal{Y}}(\tilde{\Pi}, \tilde{\mu})$, and therefore $\rho^{\mathcal{Y}}(X)$ can reach y^{EQ} . Hence, the maximum of the entropy function is achieved on the ray given by $(\bar{\rho}^{\mathcal{Y}})^{-1}(y^{\text{EQ}})$, which represents a set of the equilibrium states. Since the second law imposes that the total entropy function increases in the time evolution of the system, it will converge to a point on the equilibrium ray, depending on the initial condition and the functional form of the reaction flux $J(t)$ in Eq. (17). We should note that the equilibrium state is identified by a unique point in the density space \mathcal{X} . However, in the number space \mathfrak{X} , the equilibrium states form a ray and the equilibrium point the system converges is one of the points on the ray.

Example 4: Consider the autocatalytic motif shown in FIG. 3(a) and the intensive variables $\tilde{\Pi}$ and $\tilde{\mu}$ in the reservoir satisfy $\varphi^*(y^{\text{EQ}}) - \tilde{\Pi} = 0$. In this case, the isobaric manifold $\mathcal{I}^{\mathcal{Y}}(\tilde{\Pi}, \tilde{\mu})$ in the chemical potential space \mathcal{Y} is shown in FIG. 6(a), and y^{EQ} lies on $\mathcal{I}^{\mathcal{Y}}(\tilde{\Pi}, \tilde{\mu})$. Furthermore, the maximum of the entropy function $\Sigma^{\text{tot}}(X)$ is achieved on the ray given by $(\bar{\rho}^{\mathcal{Y}})^{-1}(y^{\text{EQ}})$ (see the right panel of FIG. 6(a)).

□

Second, we show that the system eventually shrinks if $\varphi^*(y^{\text{EQ}}) - \tilde{\Pi} < 0$. In this case, $K^{\mathcal{Y}}(y)$ is negative for all $y \in \mathcal{Y}$. Thus, on a ray in \mathfrak{X} given by $(\bar{\rho}^{\mathcal{Y}})^{-1}(y)$ for any y , the value $K^{\mathcal{Y}}(\rho^{\mathcal{Y}}(X))$ is a negative constant. In addition, $\Omega(X)$ is an increasing function on the ray because of its homogeneity. Thus, the entropy function Σ^{tot} increases when X approaches the origin along the ray. Accordingly, the maximum of the entropy function (to be more precise, the supremum of the entropy function) is located at $X = 0$; that is, the system eventually shrinks and finally vanishes.

Example 5: For the autocatalytic motif shown in FIG. 3(a) under the condition $\varphi^*(y^{\text{EQ}}) - \tilde{\Pi} < 0$, the isobaric manifold $\mathcal{I}^{\mathcal{Y}}(\tilde{\Pi}, \tilde{\mu})$ in \mathcal{Y} is shown in FIG. 6(b). In

this case, y^{EQ} does not exist on $\mathcal{I}^{\mathcal{Y}}(\tilde{\Pi}, \tilde{\mu})$. For every $y \in \mathcal{I}^{\mathcal{Y}}(\tilde{\Pi}, \tilde{\mu})$, the corresponding ray in \mathfrak{X} is given by $(\bar{\rho}^{\mathcal{Y}})^{-1}(y)$ (see the examples, y^A , y^B , y^C and the corresponding rays in \mathfrak{X} in the right panel). On each ray, the entropy function Σ^{tot} increases when X approaches the origin as shown in the right panel of FIG. 6(b).

□

Finally, we investigate the case $\varphi^*(y^{\text{EQ}}) - \tilde{\Pi} > 0$, in which the growth of the system is realized. In this case, a region $\mathfrak{R}^{\mathcal{Y}}(\tilde{\Pi}, \tilde{\mu}) \subset \mathcal{I}^{\mathcal{Y}}(\tilde{\Pi}, \tilde{\mu})$ exists such that $K^{\mathcal{Y}}(y)$ is positive:

$$\mathfrak{R}^{\mathcal{Y}}(\tilde{\Pi}, \tilde{\mu}) := \left\{ y | y \in \mathcal{I}^{\mathcal{Y}}(\tilde{\Pi}, \tilde{\mu}), K^{\mathcal{Y}}(y) > 0 \right\}. \quad (43)$$

The existence of this region is proved as follows. By defining the larger region,

$$\mathcal{Z}^{\mathcal{Y}}(\tilde{\mu}) := \left\{ y | \varphi^*(y^{\text{EQ}}) - \varphi^*(y) - \mathcal{D}^{\mathcal{Y}}[y^{\text{EQ}}|y] > 0 \right\}, \quad (44)$$

the region $\mathfrak{R}^{\mathcal{Y}}(\tilde{\Pi}, \tilde{\mu})$ can be represented by the intersection:

$$\mathfrak{R}^{\mathcal{Y}}(\tilde{\Pi}, \tilde{\mu}) = \mathcal{I}^{\mathcal{Y}}(\tilde{\Pi}, \tilde{\mu}) \cap \mathcal{Z}^{\mathcal{Y}}(\tilde{\mu}). \quad (45)$$

Since the isobaric manifold $\mathcal{I}^{\mathcal{Y}}(\tilde{\Pi}, \tilde{\mu})$ in \mathcal{Y} is the level hypersurface of $\varphi^*(y)$ specified by $\tilde{\Pi}$ (see Eq. (36)), we obtain $\mathfrak{R}^{\mathcal{Y}}(\tilde{\Pi}, \tilde{\mu}) \neq \emptyset$, only when $\tilde{\Pi} < \varphi^*(y^{\text{EQ}})$ holds (the details are shown in Appendix D). Due to the existence of the region, a ray $(\bar{\rho}^{\mathcal{Y}})^{-1}(y)$ for any $y \in \mathfrak{R}^{\mathcal{Y}}(\tilde{\Pi}, \tilde{\mu})$ also exists in \mathfrak{X} ; and, on every ray $(\bar{\rho}^{\mathcal{Y}})^{-1}(y)$, the value $K^{\mathcal{Y}}(\rho^{\mathcal{Y}}(X))$ is a positive constant. Furthermore, since $\Omega(X)$ is an increasing function on the ray, the entropy function Σ^{tot} increases when X diverges along the ray. Accordingly, the entropy function is not bounded above, and the system is growing in this case.

Example 6: Consider the autocatalytic motif shown in FIG. 3(a) and assume that $\varphi^*(y^{\text{EQ}}) - \tilde{\Pi} > 0$. The region $\mathcal{Z}^{\mathcal{Y}}(\tilde{\mu})$ in \mathcal{Y} is indicated by light purple color in the left panel of FIG. 6(c). Then, the region $\mathfrak{R}^{\mathcal{Y}}(\tilde{\Pi}, \tilde{\mu})$ is given by the intersection between the region $\mathcal{Z}^{\mathcal{Y}}(\tilde{\mu})$ and the level hypersurface (the isobaric manifold) $\mathcal{I}^{\mathcal{Y}}(\tilde{\Pi}, \tilde{\mu})$. For any $y \in \mathfrak{R}^{\mathcal{Y}}(\tilde{\Pi}, \tilde{\mu})$, the value $K^{\mathcal{Y}}(\rho^{\mathcal{Y}}(X))$ is a positive constant. Thus, on a ray $(\bar{\rho}^{\mathcal{Y}})^{-1}(y)$ in \mathfrak{X} for every $y \in \mathfrak{R}^{\mathcal{Y}}(\tilde{\Pi}, \tilde{\mu})$, the entropy function Σ^{tot} increases when X diverges along the ray.

The region $\mathcal{Z}^{\mathcal{Y}}(\tilde{\mu})$ exists irrespective of the sign of $\varphi^*(y^{\text{EQ}}) - \tilde{\Pi}$ as in FIG. 6(a, b). However, in the cases $\varphi^*(y^{\text{EQ}}) - \tilde{\Pi} \leq 0$, the intersection with the isobaric manifold $\mathcal{I}^{\mathcal{Y}}(\tilde{\Pi}, \tilde{\mu})$ does not exist.

□

The above three situations are summarized as follows:

Theorem 1 *If and only if the reservoir condition satisfies $\varphi^*(y^{\text{EQ}}) - \tilde{\Pi} = 0$, where $y^{\text{EQ}} = -\tilde{\mu}OS^{-1}$, equilibrium states exist and the system converges to one of*

them. Furthermore, if and only if $\varphi^*(y^{\text{EQ}}) - \tilde{\Pi} < 0$, the system eventually shrinks and finally vanishes. By contrast, if and only if $\varphi^*(y^{\text{EQ}}) - \tilde{\Pi} > 0$, the system is growing.

Based on physical intuition, one expects that the fate of the system is classified by a “gradient” induced by the intensive variables $(\tilde{\Pi}, \tilde{\mu})$ in the reservoir. The above theorem makes this intuition precise in the sense that $\varphi^*(y^{\text{EQ}}) - \tilde{\Pi}$ plays the role of this gradient. In fact, $\varphi^*(y^{\text{EQ}}) - \tilde{\Pi}$ is represented by the intensive variables $(\tilde{\Pi}, \tilde{\mu})$, because y^{EQ} is determined only by the chemical potential $\tilde{\mu}$ in the reservoir through Eq. (24). Furthermore, when the gradient is balanced, i.e., $\varphi^*(y^{\text{EQ}}) - \tilde{\Pi} = 0$, the system converges to an equilibrium state. By contrast, when the gradient is not balanced, i.e., $\varphi^*(y^{\text{EQ}}) - \tilde{\Pi} \neq 0$, the system never reaches an equilibrium state.

A more precise explanation of the gradient is as follows. On the one hand, the chemical reactions in the system aim to achieve the state y^{EQ} , the pressure of which is $\varphi^*(y^{\text{EQ}})$. On the other hand, the internal pressure $\varphi^*(y)$ of the system always balances with $\tilde{\Pi}$, owing to the fast dynamics. The gradient $\varphi^*(y^{\text{EQ}}) - \tilde{\Pi}$ represents the difference between them. When $\varphi^*(y^{\text{EQ}}) - \tilde{\Pi} = 0$, the target pressure $\varphi^*(y^{\text{EQ}})$ coincides with the reservoir pressure $\tilde{\Pi}$. Then, the system converges to an equilibrium state. In the case that the target pressure is smaller than $\tilde{\Pi}$ (i.e., $\varphi^*(y^{\text{EQ}}) - \tilde{\Pi} < 0$), the chemical reactions attempt to decrease the internal pressure $\varphi^*(y)$ from $\tilde{\Pi}$ in each time step, but the system immediately regains $\varphi^*(y) = \tilde{\Pi}$. This infinitesimal and instantaneous pressure gap between the system and the reservoir leads to the shrinking and the vanishing of the system. By contrast, if the target pressure is larger than $\tilde{\Pi}$ (i.e., $\varphi^*(y^{\text{EQ}}) - \tilde{\Pi} > 0$), by the same argument, the system eventually grows (expands) in each time step and finally diverges.

VI. STEADY GROWING STATE

In this section, we consider the steady growing state and evaluate the entropy production rate at the state. Since the system is assumed to grow, we focus on the case: $\varphi^*(y^{\text{EQ}}) - \tilde{\Pi} > 0$. The steady growing state x_{SG} is defined as a state such that the density $x(t) = X(t)/\Omega(t)$ is kept constant in the time evolution and $\dot{\Omega}(t)$ is positive, where the dot denotes the differentiation with time. At this state, the number of confined chemicals $X(t)$ evolves only on a ray $\bar{\rho}_{\mathcal{X}}^{-1}(x_{\text{SG}})$, because $X(t) = \Omega(t)x_{\text{SG}}$.

In order for x_{SG} to be the steady growing state, the entropy production rate at this state must be positive, $\dot{\Sigma}^{\text{tot}}(\Omega(t)x_{\text{SG}}) > 0$, and, at the same time, the volume must be increasing, i.e., $\dot{\Omega}(t) > 0$. By substituting

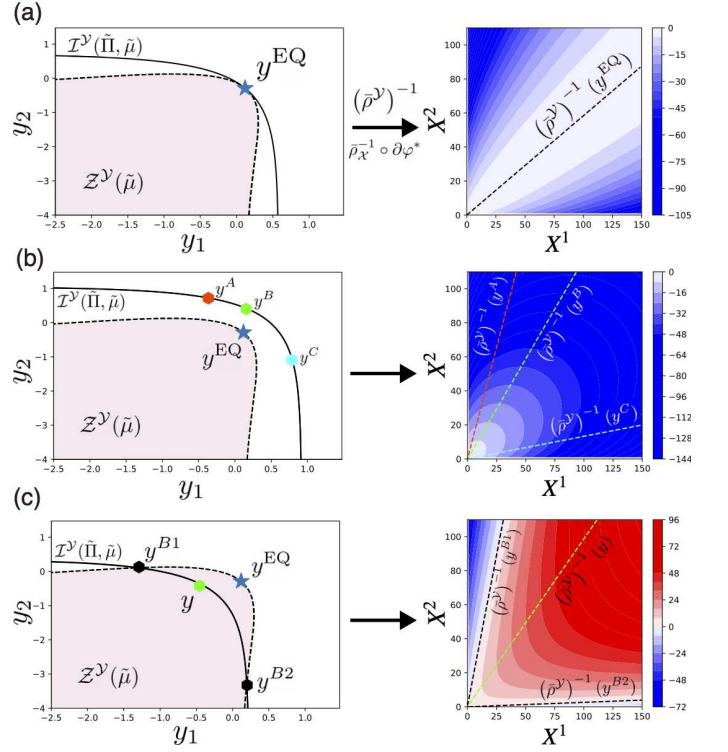


FIG. 6. For the autocatalytic motif shown in FIG. 3(a), we describe the isobaric manifold $\mathcal{I}^{\mathcal{Y}}(\tilde{\Pi}, \tilde{\mu})$ in \mathcal{Y} (left panels) and the corresponding rays in \mathfrak{X} given by the map $(\bar{\rho}^{\mathcal{Y}})^{-1} = \bar{\rho}_{\mathcal{X}}^{-1} \circ \partial\varphi^*$. The heat maps in the right panels indicate values of the entropy function Σ^{tot} (see the caption in FIG. 8 for specific values of the parameters). (a) When $\varphi^*(y^{\text{EQ}}) - \tilde{\Pi} = 0$, the point y^{EQ} lies in $\mathcal{I}^{\mathcal{Y}}(\tilde{\Pi}, \tilde{\mu})$ and $K^{\mathcal{Y}}(y^{\text{EQ}}) = 0$; for the other $y \in \mathcal{I}^{\mathcal{Y}}(\tilde{\Pi}, \tilde{\mu})$, the value of $K^{\mathcal{Y}}(y)$ is negative. Thus, the maximum $\Sigma^{\text{tot}} = 0$ is achieved on the ray given by $(\bar{\rho}^{\mathcal{Y}})^{-1}(y^{\text{EQ}})$. (b) When $\varphi^*(y^{\text{EQ}}) - \tilde{\Pi} < 0$, the point y^{EQ} does not exist on $\mathcal{I}^{\mathcal{Y}}(\tilde{\Pi}, \tilde{\mu})$ and $K^{\mathcal{Y}}(y)$ is negative for all $y \in \mathcal{I}^{\mathcal{Y}}(\tilde{\Pi}, \tilde{\mu})$. Then, on a ray in \mathfrak{X} given by $(\bar{\rho}^{\mathcal{Y}})^{-1}(y)$, the value of $K^{\mathcal{Y}}(\bar{\rho}^{\mathcal{Y}}(X))$ is negative and constant. Thus, on each ray, the entropy function Σ^{tot} increases when X approaches the origin. As a guide, we display typical points y^A , y^B and y^C , and the corresponding rays in \mathfrak{X} . (c) The region $\mathcal{Z}^{\mathcal{Y}}(\tilde{\mu})$ is indicated by light purple color in the left panel. Only when $\varphi^*(y^{\text{EQ}}) - \tilde{\Pi} > 0$, the intersection $\mathfrak{R}^{\mathcal{Y}}(\tilde{\Pi}, \tilde{\mu}) = \mathcal{I}^{\mathcal{Y}}(\tilde{\Pi}, \tilde{\mu}) \cap \mathcal{Z}^{\mathcal{Y}}(\tilde{\mu})$ appears, where $K^{\mathcal{Y}}(y)$ is positive for any $y \in \mathfrak{R}^{\mathcal{Y}}(\tilde{\Pi}, \tilde{\mu})$; i.e., within the range between y^{B1} and y^{B2} in $\mathcal{I}^{\mathcal{Y}}(\tilde{\Pi}, \tilde{\mu})$. Thus, on a ray $(\bar{\rho}^{\mathcal{Y}})^{-1}(y)$ in \mathfrak{X} for every $y \in \mathfrak{R}^{\mathcal{Y}}(\tilde{\Pi}, \tilde{\mu})$, the entropy function Σ^{tot} increases when X diverges along the ray. We also show the points y^{B1} and y^{B2} at which $K^{\mathcal{Y}}(y) = 0$, and the corresponding rays on which $\Sigma^{\text{tot}} = 0$.

$X(t) = \Omega(t)x_{\text{SG}}$ into Eq. (40), we get

$$\Sigma^{\text{tot}}(\Omega(t)x_{\text{SG}}) = \frac{\Omega(t)}{\bar{T}} \left\{ y_i^{\text{EQ}} - \partial_i \varphi(x_{\text{SG}}) \right\} x_{\text{SG}}^i, \quad (46)$$

where we use $\rho^{\mathcal{X}}(\Omega(t)x_{\text{SG}}) = x_{\text{SG}}$. By rearranging Eq.

(46) as in Eq. (41), we have

$$\Sigma^{\text{tot}}(\Omega(t) x_{\text{SG}}) = \frac{\Omega(t)}{\bar{T}} K^{\mathcal{Y}}(y^{\text{SG}}), \quad (47)$$

where $y^{\text{SG}} := \partial\varphi(x_{\text{SG}})$ and $K^{\mathcal{Y}}(y^{\text{SG}})$ is defined in Eq. (42). Since $K^{\mathcal{Y}}(y^{\text{SG}})$ is kept constant with time, the entropy production rate can be represented as

$$\dot{\Sigma}^{\text{tot}}(\Omega(t) x_{\text{SG}}) = \frac{\dot{\Omega}(t)}{\bar{T}} K^{\mathcal{Y}}(y^{\text{SG}}) > 0. \quad (48)$$

Because $\dot{\Omega}(t) > 0$ for the steady growing state, $K^{\mathcal{Y}}(y^{\text{SG}})$ must be positive. Accordingly, the chemical potential for the confined chemicals at the steady growing state, y^{SG} , must lie in the region $\mathfrak{R}^{\mathcal{Y}}(\tilde{\Pi}, \tilde{\mu}) \subset \mathcal{Y}$ (see Eqs. (43), (44) and (45)).

To clarify the region of possible x_{SG} in the density space \mathcal{X} , we map the region $\mathfrak{R}^{\mathcal{Y}}(\tilde{\Pi}, \tilde{\mu})$ to \mathcal{X} . First, we introduce the Bregman divergence on \mathcal{X} :

$$\mathcal{D}^{\mathcal{X}}[x||x'] := \{\varphi(x) - \varphi(x')\} - \partial_i \varphi(x') \{x^i - (x')^i\}. \quad (49)$$

This divergence is related to the one in \mathcal{Y} , Eq. (38), as $\mathcal{D}^{\mathcal{Y}}[y||y'] = \mathcal{D}^{\mathcal{X}}[\partial\varphi^*(y')||\partial\varphi^*(y)]$. Then, the term $K^{\mathcal{Y}}(y)$ defined by Eq. (42) is transformed as

$$K^{\mathcal{X}}(x) = \varphi^*(y^{\text{EQ}}) - \tilde{\Pi} - \mathcal{D}^{\mathcal{X}}[x||x_{\text{EQ}}], \quad (50)$$

where $x_{\text{EQ}} := \partial\varphi^*(y^{\text{EQ}})$. Thus, the region in the density space \mathcal{X} can be represented as

$$\begin{aligned} \mathfrak{R}^{\mathcal{X}}(\tilde{\Pi}, \tilde{\mu}) &:= \partial\varphi^*(\mathfrak{R}^{\mathcal{Y}}) \\ &= \{x|x \in \mathcal{I}^{\mathcal{X}}(\tilde{\Pi}, \tilde{\mu}), K^{\mathcal{X}}(x) > 0\}. \end{aligned} \quad (51)$$

Rewriting this region as the intersection of two submanifolds as in Eq. (45), we obtain

$$\begin{aligned} \mathfrak{R}^{\mathcal{X}}(\tilde{\Pi}, \tilde{\mu}) &:= \partial\varphi^*(\mathfrak{R}^{\mathcal{Y}}) = \partial\varphi^*(\mathcal{I}^{\mathcal{Y}}) \cap \partial\varphi^*(\mathcal{Z}^{\mathcal{Y}}) \\ &= \mathcal{I}^{\mathcal{X}}(\tilde{\Pi}, \tilde{\mu}) \cap \mathcal{Z}^{\mathcal{X}}(\tilde{\mu}), \end{aligned} \quad (52)$$

where the region $\mathcal{Z}^{\mathcal{X}}(\tilde{\mu})$ in \mathcal{X} is represented as

$$\mathcal{Z}^{\mathcal{X}}(\tilde{\mu}) = \{x|x^i \{\partial_i \varphi(x_{\text{EQ}}) - \partial_i \varphi(x)\} > 0\}. \quad (53)$$

The argument in this section is summarized by the following theorem:

Theorem 2 *When $\varphi^*(y^{\text{EQ}}) - \tilde{\Pi} > 0$ and a steady growing state x_{SG} exists, the state x_{SG} must lie in the region $\mathfrak{R}^{\mathcal{X}}(\tilde{\Pi}, \tilde{\mu})$. Then, the entropy production rate at the state x_{SG} is represented as*

$$\begin{aligned} \dot{\Sigma}_{\text{SG}}^{\text{tot}}(t) &= \frac{\dot{\Omega}(t)}{\bar{T}} K^{\mathcal{X}}(x_{\text{SG}}) \\ &= \frac{\dot{\Omega}(t)}{\bar{T}} \{\varphi^*(y^{\text{EQ}}) - \tilde{\Pi}\} - \frac{\dot{\Omega}(t)}{\bar{T}} \mathcal{D}^{\mathcal{X}}[x_{\text{SG}}||x_{\text{EQ}}]. \end{aligned} \quad (54)$$

The above theorem only identifies the region of possible steady growing states. The existence and uniqueness of such states are not guaranteed, and which states would be chosen in this region is not determined. These details can be analyzed and determined once we specify the functional form of the reaction flux $J(t)$. For example, we assume that $J(t)$ of the CRS given in FIG. 3(a) obeys mass action kinetics and observe that the steady growing state exists as in FIG. 3(d). However, if the functional form of the kinetic law is different from mass action, the existence of the steady growing state is not guaranteed even in the CRS.

By rearranging Eq. (54), we obtain

$$\bar{T} \frac{\dot{\Sigma}_{\text{SG}}^{\text{tot}}(t)}{\dot{\Omega}(t)} = \{\varphi^*(y^{\text{EQ}}) - \tilde{\Pi}\} - \mathcal{D}^{\mathcal{X}}[x_{\text{SG}}||x_{\text{EQ}}]. \quad (55)$$

The left hand side of this expression represents the thermodynamic cost for the volume growth, whereas the right hand side can be interpreted as follows. The first term represents the external contribution, which is the gradient $\varphi^*(y^{\text{EQ}}) - \tilde{\Pi}$ induced by the reservoir. The second term characterizes the internal contribution, which is the Bregman divergence $\mathcal{D}^{\mathcal{X}}[x_{\text{SG}}||x_{\text{EQ}}]$ from the equilibrium state x_{EQ} to the steady growing state x_{SG} . It gives the total entropy increment during an isochoric relaxation $x_{\text{SG}} \rightarrow x_{\text{EQ}}$ (see Ref. [51] for details). This fact suggests to interpret the second term as the relaxation contribution by the chemical reactions in the system. Moreover, in the right hand side, only the steady growing state x_{SG} depends on the reaction flux $J(t)$. When one designs the reaction flux $J(t)$ to optimize the thermodynamic cost, the expression, Eq. (55), may play an important role.

Example 7: For the example shown in FIG. 6(c), in which $\varphi^*(y^{\text{EQ}}) - \tilde{\Pi} > 0$ holds, the region $\mathcal{Z}^{\mathcal{X}}(\tilde{\mu})$ exists in \mathcal{X} , as indicated by the light purple color in FIG. 7. Under the ideal gas assumption, the isobaric manifold $\mathcal{I}^{\mathcal{X}}(\tilde{\Pi}, \tilde{\mu})$ is a simplex in \mathcal{X} as we will show in the next section. Then, the intersection $\mathfrak{R}^{\mathcal{X}}(\tilde{\Pi}, \tilde{\mu}) = \mathcal{I}^{\mathcal{X}}(\tilde{\Pi}, \tilde{\mu}) \cap \mathcal{Z}^{\mathcal{X}}(\tilde{\mu})$ exists as the dashed red rectangle in FIG. 7, where $K^{\mathcal{X}}(x)$ is positive for any $x \in \mathfrak{R}^{\mathcal{X}}(\tilde{\Pi}, \tilde{\mu})$. If a steady growing state x_{SG} exists, it must be in the region $\mathfrak{R}^{\mathcal{X}}(\tilde{\Pi}, \tilde{\mu})$. \square

VII. IDEAL GAS

In this section, we demonstrate our framework for CRSs under the ideal gas assumption. To be more precise, we assume that both the system and the reservoir are composed of ideal gas.

To write down Theorem 1 in this situation, we first evaluate the full grand potential density $\varphi^*(y)$. The form of the Helmholtz free-energy density for the ideal gas is

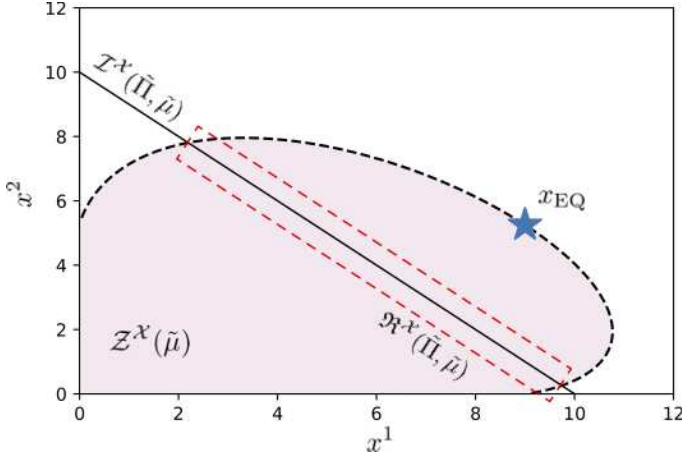


FIG. 7. The isobaric manifold $I^{\mathcal{X}}(\tilde{\Pi}, \tilde{\mu})$ in \mathcal{X} , corresponding to the case in FIG. 6(c). If the system is composed of ideal gas, then $I^{\mathcal{X}}(\tilde{\Pi}, \tilde{\mu})$ is a simplex. The region $Z^{\mathcal{X}}(\tilde{\mu})$ is indicated by light purple color. The region $\mathfrak{R}^{\mathcal{X}}(\tilde{\Pi}, \tilde{\mu})$ is the intersection between $I^{\mathcal{X}}(\tilde{\Pi}, \tilde{\mu})$ and $Z^{\mathcal{X}}(\tilde{\mu})$, which is enclosed by the dashed red rectangle. If a steady growing state exists, it must be in this region.

known as

$$f[\tilde{T}; n, x] = n^m \mu_m^o(\tilde{T}) + R\tilde{T} \sum_m \{n^m \log n^m - n^m\} + x^i \nu_i^o(\tilde{T}) + R\tilde{T} \sum_i \{x^i \log x^i - x^i\}, \quad (56)$$

where R represents the gas constant; $\mu^o(\tilde{T}) = \{\mu_m^o(\tilde{T})\}$ and $\nu^o(\tilde{T}) = \{\nu_i^o(\tilde{T})\}$ denote the standard chemical potentials of the open and confined chemicals, respectively. Since the partial grand potential density $\varphi[\tilde{T}, \tilde{\mu}; x]$ can be represented by a variant of the Legendre transformation:

$$\varphi[\tilde{T}, \tilde{\mu}; x] := \min_n \{f[\tilde{T}; n, x] - \tilde{\mu}_m n^m\}, \quad (57)$$

we get

$$\varphi[\tilde{T}, \tilde{\mu}; x] = \varphi(x) = x^i \nu_i^o(\tilde{T}) + R\tilde{T} \sum_i \{x^i \log x^i - x^i\} - R\tilde{T} \sum_m e^{\{\tilde{\mu}_m - \mu_m^o(\tilde{T})\}/R\tilde{T}}. \quad (58)$$

Also, from the Legendre transformation, Eq. (34), the full grand potential density $\varphi^*(y)$ can be expressed as

$$\varphi^*(y) = R\tilde{T} \sum_i e^{\{y_i - \nu_i^o(\tilde{T})\}/R\tilde{T}} + R\tilde{T} \sum_m e^{\{\tilde{\mu}_m - \mu_m^o(\tilde{T})\}/R\tilde{T}}. \quad (59)$$

Furthermore, since we have assumed that the reservoir also consists of the ideal gas, the chemical potential $\tilde{\mu}$ can be represented as

$$\tilde{\mu}_m = \mu_m^o(\tilde{T}) + R\tilde{T} \log \tilde{n}^m, \quad (60)$$

where $\tilde{n} = \{\tilde{n}^m\}$ is the density of the open chemicals in the reservoir. In addition, for notational simplicity, we define the standard density for the confined chemicals as $x_o^i := e^{-\nu_i^o(\tilde{T})/R\tilde{T}}$ [62]. Then, Eq. (59) is rearranged to

$$\varphi^*(y) = R\tilde{T} \sum_i x_o^i e^{y_i/R\tilde{T}} + R\tilde{T} \sum_m \tilde{n}^m. \quad (61)$$

Next, we calculate the gradient $\varphi^*(y^{\text{EQ}}) - \tilde{\Pi}$ in Theorem 1. By defining the standard density for the open chemicals as $n_o^m := e^{-\mu_m^o(\tilde{T})/R\tilde{T}}$, we get $\tilde{\mu}_m = R\tilde{T} \log(\tilde{n}^m/n_o^m)$. Hence, $y^{\text{EQ}} = -\tilde{\mu}OS^{-1}$ in Eq. (24) can be rewritten as

$$y_i^{\text{EQ}} = R\tilde{T} \prod_m \log\left(\frac{n_o^m}{\tilde{n}^m}\right)^{(OS^{-1})_i^m}. \quad (62)$$

By substituting y^{EQ} into Eq. (61), we obtain

$$\varphi^*(y^{\text{EQ}}) - \tilde{\Pi} = R\tilde{T} \sum_i \prod_m x_o^i \left(\frac{n_o^m}{\tilde{n}^m}\right)^{(OS^{-1})_i^m} - \left(\tilde{\Pi} - R\tilde{T} \sum_m \tilde{n}^m\right). \quad (63)$$

Here, we note that the second line in Eq. (63) represents the partial pressure that is produced by compositions other than the open chemicals in the reservoir. For the ideal gas, Eq. (63) determines the fate of the system.

Finally, we specify Theorem 2 for the ideal gas. The isobaric manifold $I^{\mathcal{X}}(\tilde{\Pi}, \tilde{\mu})$ in Eq. (32) is rewritten as

$$I^{\mathcal{X}}(\tilde{\Pi}, \tilde{\mu}) := \left\{ x \mid R\tilde{T} \sum_i x^i - \left(\tilde{\Pi} - R\tilde{T} \sum_m \tilde{n}^m\right) = 0 \right\}, \quad (64)$$

which implies the equation of state, $\tilde{\Pi} = R\tilde{T}(\sum_i x^i + \sum_m \tilde{n}^m)$, and defines a simplex in the density space \mathcal{X} . Also, by using Eq. (58), the region $Z^{\mathcal{X}}(\tilde{\mu})$ in Eq. (53) can be expressed as

$$Z^{\mathcal{X}}(\tilde{\mu}) = \left\{ x \mid R\tilde{T} \sum_i x^i \log\left(\frac{x_{\text{EQ}}^i}{x^i}\right) > 0 \right\}, \quad (65)$$

where $x_{\text{EQ}}^i = \partial \varphi^*(y^{\text{EQ}}) = x_o^i e^{y_i^{\text{EQ}}/R\tilde{T}}$. Note that $\sum_i x^i \log(x_{\text{EQ}}^i/x^i)$ can be negative because x and x_{EQ} are not normalized. Thus, the region $\mathfrak{R}^{\mathcal{X}}(\tilde{\Pi}, \tilde{\mu})$ is given by the intersection between Eqs. (64) and (65). In addition, the Bregman divergence in the density space \mathcal{X} , Eq. (49), reduces to the generalized Kullback-Leibler divergence [43–45, 50]:

$$D^{\mathcal{X}}[x \parallel x_{\text{EQ}}] = R\tilde{T} \sum_i \left[x^i \log \frac{x^i}{x_{\text{EQ}}^i} - \{x^i - x_{\text{EQ}}^i\} \right]. \quad (66)$$

Accordingly, the entropy production rate $\dot{\Sigma}_{\text{SG}}^{\text{tot}}(t)$ is evaluated by substituting Eqs. (63) and (66) into Eq. (54). To

obtain the entropy production rate in Eq. (54), we still need to calculate the growth rate $\hat{\Omega}(t)$ and the steady growing state x_{SG} . To compute them, we must determine the functional form of the reaction flux $J(t)$. We should recall that Theorem 2 only identifies the region of possible steady growing states x_{SG} .

Example 8: The geometric representations of the examples shown in FIG. 6 and 7 are obtained as follows for the ideal gas. Before presenting the geometry, we list the given parameters: (1) the stoichiometric matrices S and O ; (2) the intensive variables $(\tilde{T}, \tilde{\Pi}, \tilde{\mu})$ in the reservoir; (3) the standard densities $\{n_o, x_o\}$ and the standard chemical potentials $\{\mu^o(\tilde{T}), \nu^o(\tilde{T})\}$ for the open and the confined chemicals, which are related to each other as $n_o^m = e^{-\mu_m^o(\tilde{T})/R\tilde{T}}$ and $x_o^i = e^{-\nu_i^o(\tilde{T})/R\tilde{T}}$; (4) the density \tilde{n} for the open chemicals in the reservoir, which leads to the chemical potential as $\tilde{\mu}_m = \mu^o(\tilde{T}) + R\tilde{T} \log \tilde{n}^m$.

First, we determine the isobaric manifolds $\mathcal{I}^{\mathcal{X}}(\tilde{\Pi}, \tilde{\mu})$ and $\mathcal{I}^{\mathcal{Y}}(\tilde{\Pi}, \tilde{\mu})$. By using the given \tilde{T} , $\tilde{\Pi}$ and \tilde{n} , we obtain the isobaric manifold $\mathcal{I}^{\mathcal{X}}(\tilde{\Pi}, \tilde{\mu})$ in the density space \mathcal{X} from Eq. (64) as the simplex in FIG. 7. Also, we can describe the isobaric manifold $\mathcal{I}^{\mathcal{Y}}(\tilde{\Pi}, \tilde{\mu})$ in the chemical potential space \mathcal{Y} by substituting Eq. (61) into Eq. (36), as shown in the left panels of FIG. 6.

Second, we determine the regions $\mathcal{Z}^{\mathcal{X}}(\tilde{\mu})$ and $\mathcal{Z}^{\mathcal{Y}}(\tilde{\mu})$. By employing Eq. (62), we can calculate y^{EQ} ; and by applying the map $\partial^i \varphi^*(y) = x_o^i e^{y_i/R\tilde{T}}$ to y^{EQ} , we get x_{EQ} . The substitution of x_{EQ} into Eq. (65) leads to $\mathcal{Z}^{\mathcal{X}}(\tilde{\mu})$ (see the light purple region in FIG. 7). We also obtain $\mathcal{Z}^{\mathcal{Y}}(\tilde{\mu})$ by substituting Eqs. (61) and (38) into Eq. (44) (see the light purple regions in the left panels of FIG. 6).

Third, we determine the region $\mathfrak{R}^{\mathcal{X}}(\tilde{\Pi}, \tilde{\mu})$ for possible steady growing states x_{SG} by Eq. (52). It is given by the intersection between $\mathcal{I}^{\mathcal{X}}(\tilde{\Pi}, \tilde{\mu})$ and $\mathcal{Z}^{\mathcal{X}}(\tilde{\mu})$, i.e., the dashed red rectangle in FIG. 7.

Finally, the entropy function $\Sigma^{\text{tot}}(X)$ on \mathfrak{X} is calculated from Eq. (41). Here, the volume $\Omega(X)$ is obtained from Eq. (27) with Eq. (58), i.e., from the equation of state:

$$\Omega(X) = \frac{R\tilde{T} \sum_i X^i}{\tilde{\Pi} - R\tilde{T} \sum_m \tilde{n}^m}. \quad (67)$$

Also, the map $\rho^{\mathcal{Y}}(X)$ can be calculated as

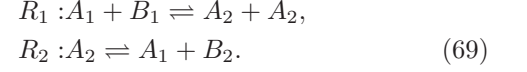
$$\rho_i^{\mathcal{Y}}(X) = \partial_i \varphi \circ \rho_{\mathcal{X}}(X) = R\tilde{T} \log \left(\frac{X^i}{\Omega(X) x_o^i} \right). \quad (68)$$

The heat maps of the right panels of FIG. 6 are plotted using these equations. \square

VIII. NUMERICAL VERIFICATION

To numerically verify our theory, we deal with the minimal motif of autocatalytic cycles as given in Sec. II, where we assume ideal gas conditions and mass action kinetics.

The chemical equations of the motif have been represented by two reactions R_1 and R_2 that involve two confined chemicals $A = (A_1, A_2)$ and two open chemicals $B = (B_1, B_2)$:



Also, the stoichiometric matrices are

$$S = \begin{matrix} & R_1 & R_2 \\ \begin{matrix} A_1 \\ A_2 \end{matrix} & \begin{pmatrix} -1 & 1 \\ 2 & -1 \end{pmatrix} \end{matrix}, \quad O = \begin{matrix} & R_1 & R_2 \\ \begin{matrix} B_1 \\ B_2 \end{matrix} & \begin{pmatrix} -1 & 0 \\ 0 & 1 \end{pmatrix} \end{matrix}. \quad (70)$$

The regularity of the matrix S is checked as $\det[S] = -1 \neq 0$. Denoting the number of $A = (A_1, A_2)$ by $X = (X^1, X^2)$, the reaction dynamics for the confined chemicals is written as

$$\frac{dX^i}{dt} = S_r^i J^r(t). \quad (71)$$

Furthermore, we assume mass action kinetics for the reaction flux $J(t)$:

$$\begin{aligned} J^1(t) &= w_+^1 X^1 \frac{N^1}{\Omega} - w_-^1 X^2 \frac{X^2}{\Omega}, \\ J^2(t) &= w_+^2 X^2 - w_-^2 X^1 \frac{N^2}{\Omega}, \end{aligned} \quad (72)$$

where $N = (N^1, N^2)$ denotes the number of $B = (B_1, B_2)$ in the system. The rate constants w_+^r and w_-^r satisfy

$$\log \frac{w_+^r}{w_-^r} = -\frac{1}{R\tilde{T}} \left\{ \nu_i^o(\tilde{T}) S_r^i + \mu_m^o(\tilde{T}) O_r^m \right\}, \quad (73)$$

which is known as the local detailed balance condition [43, 44, 51, 52, 58].

To solve Eq. (71), we need to elucidate the behavior of N and Ω . For the ideal gas, the density N/Ω of the open chemicals in the system coincides with the density \tilde{n} in the reservoir, which is a constant in time (see Appendix E). In addition, Ω is given by the equation of state as Eq. (67). Thus, Eq. (72) can be rearranged as

$$\begin{aligned} J^1(t) &= \hat{w}_+^1 X^1 - \hat{w}_-^1 \frac{(X^2)^2}{\Omega(X)}, \\ J^2(t) &= \hat{w}_+^2 X^2 - \hat{w}_-^2 X^1, \end{aligned} \quad (74)$$

where we absorb the constant densities of the open chemicals, N^m/Ω , into the rate constants as \hat{w}_+^r and \hat{w}_-^r . Then,

the local detailed balance condition in Eq. (73) can be written as

$$\log \frac{\hat{w}_+^r}{\hat{w}_-^r} = -\frac{1}{RT} \left\{ \nu_i^0(\tilde{T}) S_r^i + \tilde{\mu}_m O_r^m \right\}, \quad (75)$$

and, for our specific example, it reduces to

$$\frac{\hat{w}_+^1}{\hat{w}_-^1} = \frac{x_o^2 x_o^2 \tilde{n}^1}{x_o^1 n_o^1}, \quad \frac{\hat{w}_+^2}{\hat{w}_-^2} = \frac{x_o^1 n_o^2}{x_o^2 \tilde{n}^2}. \quad (76)$$

In FIG. 8, we show the trajectories of the system, from two initial conditions 1 and 2, in the spaces \mathfrak{X} , \mathcal{X} and \mathcal{Y} .

When the equality $\varphi^*(y^{\text{EQ}}) - \tilde{\Pi} = 0$ holds (see FIG. 8(a)), the total entropy function is increasing as the system moves on \mathfrak{X} and converges to a point, denoted by the square, on the equilibrium ray. The point depends on the initial conditions. In the spaces \mathcal{X} and \mathcal{Y} (FIG. 8(b, c)), the system moves on the isobaric manifolds $\mathcal{I}^{\mathcal{X}}(\tilde{\Pi}, \tilde{\mu})$ and $\mathcal{I}^{\mathcal{Y}}(\tilde{\Pi}, \tilde{\mu})$, respectively, and converges to the equilibrium points x_{EQ} and y^{EQ} , irrespective of the initial conditions.

When $\varphi^*(y^{\text{EQ}}) - \tilde{\Pi} < 0$ (see FIG. 8(d)), the system first converges to a ray, and then moves on the ray toward the origin of \mathfrak{X} , driven by the increase of the entropy function. In the spaces \mathcal{X} and \mathcal{Y} (FIG. 8(e, f)), the system moves on the isobaric manifolds $\mathcal{I}^{\mathcal{X}}(\tilde{\Pi}, \tilde{\mu})$ and $\mathcal{I}^{\mathcal{Y}}(\tilde{\Pi}, \tilde{\mu})$, respectively, and converges to the points denoted by the squares. These points correspond to the ray on which the system moves toward the origin in \mathfrak{X} . Therefore, the system finally vanishes.

Finally, when $\varphi^*(y^{\text{EQ}}) - \tilde{\Pi} > 0$ (FIG. 8(g)), the system first converges to a ray, and then moves on the ray away from the origin of \mathfrak{X} with the increase of the entropy function. In the spaces \mathcal{X} and \mathcal{Y} (FIG. 8(h, i)), the system moves on the isobaric manifolds $\mathcal{I}^{\mathcal{X}}(\tilde{\Pi}, \tilde{\mu})$ and $\mathcal{I}^{\mathcal{Y}}(\tilde{\Pi}, \tilde{\mu})$, respectively, and converges to points x_{SG} and $y^{\text{SG}} = \partial\varphi(x_{\text{SG}})$ denoted by the squares. These points correspond to the ray on which the system moves in \mathfrak{X} , and are indeed located in $\mathfrak{X}^{\mathcal{X}}(\tilde{\Pi}, \tilde{\mu})$ and $\mathfrak{X}^{\mathcal{Y}}(\tilde{\Pi}, \tilde{\mu})$ (see also FIG. 6(c) and FIG. 7).

IX. SUMMARY AND DISCUSSION

We have established the thermodynamics of growing chemical reaction systems (CRSs) by employing Hessian and projective geometry. In this work, we have classified the environmental conditions to distinguish the fate of the CRSs. Furthermore, under the growing condition, we have identified the region in the density space where a steady growing state can exist. We have also evaluated the entropy production rate in this state. It is emphasized again that our results are derived by a general thermodynamic structure without assuming any specific thermodynamic potentials or reaction kinetics; i.e., they are obtained based solely on the second law of thermodynamics.

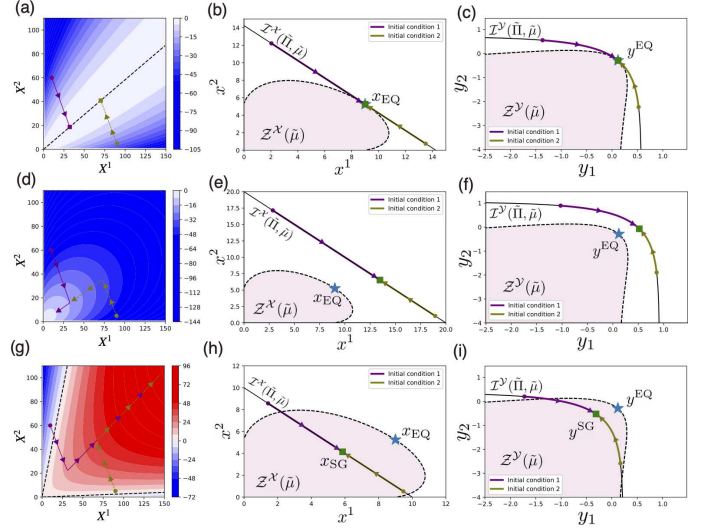


FIG. 8. Trajectories of the system in the spaces of the number of confined chemicals \mathfrak{X} (left panel; a, d, g), the density space \mathcal{X} (middle panel; b, e, h), and the chemical potential space \mathcal{Y} (right panel; c, f, i) for different pressures $\tilde{\Pi}$ satisfying (top; a,b,c) $\varphi^*(y^{\text{EQ}}) - \tilde{\Pi} = 0$, (middle; d,e,f) $\varphi^*(y^{\text{EQ}}) - \tilde{\Pi} = -5.75$, (bottom; g,h,i) $\varphi^*(y^{\text{EQ}}) - \tilde{\Pi} = 4.25$. For our simulation, $x_{\text{EQ}} = (9, 5.25)$ and $y^{\text{EQ}} = (0.118, -0.288)$. The parameters of the simulation are fixed as follows: $R = \tilde{T} = 1$, $x_o^1 = 8$, $x_o^2 = 7$, $n_o^1 = 2$, $\tilde{n}^1 = 1$, $n_o^2 = 3$, $\tilde{n}^2 = 2$, $\hat{w}_+^1 = \hat{w}_-^1 = 1$. The rate constants of forward reactions, \hat{w}_+^1 and \hat{w}_+^2 , are computed by Eq. (76). For the initial conditions 1 and 2, we set $(X_1, X_2) = (10, 60)$ and $(90, 5)$, respectively.

In this work, we have assumed that the stoichiometric matrix S is regular. This implies that the system can always relax to a chemical equilibrium state when the volume is fixed, i.e., in the isochoric situation [51]. In other words, the system never reaches a state that continuously produces entropy with constant volume, namely, the conventional nonequilibrium steady state (NESS) [43–50]. Accordingly, the nonequilibrium states treated here, notably the steady growing state, are realized due to the change of the volume. This nonequilibrium state with changing volume originates in the extensivity of thermodynamics and should be distinct from the conventional NESS with constant volume.

If the matrix S has a nontrivial right null space ($\dim \text{Ker}[S] \neq 0$), the system may relax to the NESS even for a constant volume situation. Such a nongrowing but nonequilibrium state is also biologically relevant, for example, the stationary phase of cells [12, 63–66]. It is a major challenge for the future to clarify how the nonequilibrium state caused by volume growth and the conventional NESS without growth are compatible and related to each other.

By contrast, if the matrix S has a nontrivial left null space ($\dim \text{Ker}[S^T] \neq 0$), the system has conservation laws [43, 44, 51, 52]. In our framework, it remains an

open problem whether steady growth of the system is possible and realized with the conservation laws.

In our setup, we have ignored the tension of the membrane and assumed that it never bursts (see the caption in FIG. 1). However, the membrane does have tension in actual situations. Even for such cases, our framework can be applied by effectively incorporating the tension into the pressure $\tilde{\Pi}$. Furthermore, in biological cells, the membrane molecules themselves are produced and supplied by the intracellular CRS. In this case, the tension is coupled and changes with the CRS, and therefore the effective $\tilde{\Pi}$ changes with time. Accordingly, our theoretical framework needs to be extended further.

Our theory surely serves as the basis of all these extensions, which are important for considering actual and experimental situations of growing protocells or biological cells and also for establishing the physics of self-replicating systems.

ACKNOWLEDGEMENT

The authors thank Kento Nakamura and Genta Chiba for fruitful discussion. This research is supported by JSPS KAKENHI Grant Numbers 19H05799 and 21K21308, and by JST CREST JPMJCR2011 and JPMJCR1927.

Appendix A

In this appendix, we introduce the concept of minimal motifs for growing systems called ‘‘autocatalytic cores’’. It was originally proposed in Ref. [26] to determine whether a subnetwork embedded in a larger chemical reaction network can be autocatalytic. Furthermore, the authors of Ref. [26] have shown that the regularity of the stoichiometric matrices of the motifs plays an essential role to identify such cores, by providing the following theorem:

Theorem 3 *If a chemical reaction network is an autocatalytic core, its stoichiometric matrix S for the confined chemicals must be regular.*

In the following part, we will briefly review the proof of their theorem (Theorem 3) with our notations.

First, we mathematically define several conditions for a stoichiometric matrix S . All of the following definitions are introduced in Ref. [26]. The matrix S is *productive*, if $\text{Im}[S] \cap \mathbb{R}_{>0}^{\mathcal{N}_X} \neq \emptyset$. The matrix S is *autonomous*, if all column vectors of S contain both strictly negative and strictly positive elements. The matrix S is an *autocatalytic core*, if S is both productive and autonomous; in addition, S satisfies the following condition: if we remove a row or a column vector from S , the reduced matrix of S is not both productive and autonomous. With this

final condition, the matrix S is referred to as minimal, because it does not contain any smaller motifs satisfying both productivity and autonomy.

Furthermore, we prepare the following terms for the proof: If a species is the only reactant of a reaction, we call it the *solitary reactant* of the reaction; otherwise, we call it a *coreactant* of the reaction.

The above definitions immediately lead to the following lemmas. **(Lemma 1)** We can remove an arbitrary column vector from S , while preserving autonomy. **(Lemma 2)** We can remove an arbitrary row vector from S , while preserving productivity. **(Lemma 3)** If a species exists such that it is not the solitary reactant for all reactions in S , we can remove the row vector corresponding to the species, while preserving productivity and autonomy.

With the above definitions and lemmas, we now prove Theorem 3. Consider an autocatalytic core S of size $\mathcal{N}_X \times \mathcal{N}_R$ with rank λ . If we assume $\dim \text{Ker}[S] \neq 0$, we can remove a column vector, while preserving $\text{Im}[S]$, that is, preserving productivity. This contradicts the condition that an autocatalytic core S is minimal. Thus, $\dim \text{Ker}[S]$ must be zero, and therefore we have $\lambda = \mathcal{N}_R$. Furthermore, for every species, some reactions exist such that the species is the solitary reactant of the reactions. Otherwise, because of Lemma 3, we can remove a row vector and this contradicts the condition again that an autocatalytic core S is minimal. Thus, we get $\mathcal{N}_X \leq \mathcal{N}_R$. Since $\lambda \leq \mathcal{N}_X, \mathcal{N}_R$, it follows that $\lambda = \mathcal{N}_X = \mathcal{N}_R$. This means that S is regular.

Appendix B

In this appendix, we derive the effective slow dynamics by employing the second law of thermodynamics.

Since we have assumed $J_E(t), J_\Omega(t), J_D \gg J(t)$, we can ignore the reaction flux $J(t)$ in Eqs. (3) and (4) for the fast time scale. Then, we get the effective fast dynamics as

$$\begin{aligned} \frac{dE}{dt} &= J_E(t), \quad \frac{d\Omega}{dt} = J_\Omega(t), \quad \frac{dN^m}{dt} = J_D^m(t), \\ \frac{d\tilde{E}}{dt} &= -J_E(t), \quad \frac{d\tilde{\Omega}}{dt} = -J_\Omega(t), \quad \frac{d\tilde{N}^m}{dt} = -J_D^m(t). \end{aligned} \quad (77)$$

The formal solution of Eq. (77) with the initial condition $(E_0, \Omega_0, N_0, \tilde{E}_0, \tilde{\Omega}_0, \tilde{N}_0)$ can be represented as

$$\begin{aligned} E(t) &= E_0 + \Delta_E(t), \quad \Omega(t) = \Omega_0 + \Delta_\Omega(t), \\ N^m(t) &= N_0^m + \Delta_N^m(t), \quad \tilde{E}(t) = \tilde{E}_0 - \Delta_E(t), \\ \tilde{\Omega}(t) &= \tilde{\Omega}_0 - \Delta_\Omega(t), \quad \tilde{N}^m(t) = \tilde{N}_0^m - \Delta_N^m(t), \end{aligned} \quad (78)$$

where $(\Delta_E(t), \Delta_\Omega(t), \Delta_N(t))$ are the integrals of the flux functions $(J_E(t), J_\Omega(t), J_D(t))$ with the initial condition $J_E(0) = J_\Omega(0) = J_D(0) = 0$. Note that the number of the confined chemicals, $X(t)$, is a constant in this dynamics.

By substituting this solution into Eq. (1), we have the time evolution of the total entropy as

$$\begin{aligned} \Sigma^{\text{tot}}(\Delta_E, \Delta_\Omega, \Delta_N) &= \Sigma[E_0 + \Delta_E, \Omega_0 + \Delta_\Omega, N_0 + \Delta_N, X] \\ &\quad - \frac{1}{\tilde{T}} \Delta_E - \frac{\tilde{\Pi}}{\tilde{T}} \Delta_\Omega + \frac{\tilde{\mu}_m}{\tilde{T}} \Delta_N^m + \text{const.}, \end{aligned} \quad (79)$$

where we use properties of the reservoir; i.e., $\Delta_E(t) \ll \tilde{E}_0$, $\Delta_\Omega(t) \ll \tilde{\Omega}_0$, $\Delta_N(t) \ll \tilde{N}_0$, and the Taylor expansion for $\tilde{\Sigma}_{\tilde{T}, \tilde{\Pi}, \tilde{\mu}}$; we also use the thermodynamic relations: $\partial \tilde{\Sigma}_{\tilde{T}, \tilde{\Pi}, \tilde{\mu}} / \partial \tilde{E} = 1/\tilde{T}$, $\partial \tilde{\Sigma}_{\tilde{T}, \tilde{\Pi}, \tilde{\mu}} / \partial \tilde{\Omega} = \tilde{\Pi}/\tilde{T}$ and $\partial \tilde{\Sigma}_{\tilde{T}, \tilde{\Pi}, \tilde{\mu}} / \partial \tilde{N}^m = -\tilde{\mu}_m/\tilde{T}$. In addition, we abbreviate the constant term $\tilde{\Sigma}_{\tilde{T}, \tilde{\Pi}, \tilde{\mu}}[\tilde{E}_0, \tilde{\Omega}_0, \tilde{N}_0]$ to ‘‘const.’’. According to the second law, the system must climb up the landscape defined by the concave function $\Sigma^{\text{tot}}(\Delta_E, \Delta_\Omega, \Delta_N)$ in the time evolution, and finally converge to its maximum, which is called the equilibrium state. Hence, we get

$$\begin{aligned} (\Delta_E, \Delta_\Omega, \Delta_N) &\rightarrow \left((\Delta_E)_{\text{QEQ}}, (\Delta_\Omega)_{\text{QEQ}}, (\Delta_N)_{\text{QEQ}} \right) \\ &= \arg \max_{\Delta_E, \Delta_\Omega, \Delta_N} \Sigma^{\text{tot}}(\Delta_E, \Delta_\Omega, \Delta_N), \end{aligned} \quad (80)$$

where $(\cdot)_{\text{QEQ}}$ represents the value at the equilibrium state of the fast dynamics. However, we call this the quasi-equilibrium state, because we later consider the slow dynamics. By using the argument shift $E = E_0 + \Delta_E$, $\Omega = \Omega_0 + \Delta_\Omega$, $N = N_0 + \Delta_N$ and taking Eq. (79) into account, we get the extensive variables at the quasi-equilibrium state as

$$\begin{aligned} (E_{\text{QEQ}}, \Omega_{\text{QEQ}}, N_{\text{QEQ}}) &= \arg \max_{E, \Omega, N} \left\{ \Sigma[E, \Omega, N, X] - \frac{1}{\tilde{T}} E - \frac{\tilde{\Pi}}{\tilde{T}} \Omega + \frac{\tilde{\mu}_m}{\tilde{T}} N^m \right\}. \end{aligned} \quad (81)$$

The above characterization of the quasi-equilibrium state by the variational form, Eq. (81), can be rearranged by introducing thermodynamic potentials as follows. First, we define the Helmholtz free energy as

$$F[\tilde{T}; \Omega, N, X] := \min_E \left\{ E - \tilde{T} \Sigma[E, \Omega, N, X] \right\}. \quad (82)$$

Second, by using the Helmholtz free energy, we introduce the partial grand potential:

$$\Phi[\tilde{T}, \tilde{\mu}; \Omega, X] := \min_N \left\{ F[\tilde{T}; \Omega, N, X] - \tilde{\mu}_m N^m \right\}. \quad (83)$$

With the above two thermodynamic potentials, we can reformulate the variational form, Eq. (81), as

$$\Omega_{\text{QEQ}}(X) = \arg \min_{\Omega} \left\{ \Phi[\tilde{T}, \tilde{\mu}; \Omega, X] + \tilde{\Pi} \Omega \right\}. \quad (84)$$

The other two values, E_{QEQ} and N_{QEQ} , can be computed as follows. Since the equality,

$$\begin{aligned} \Phi[\tilde{T}, \tilde{\mu}; \Omega_{\text{QEQ}}, X] &= -\tilde{T} \Sigma[E_{\text{QEQ}}, \Omega_{\text{QEQ}}, N_{\text{QEQ}}, X] \\ &\quad + E_{\text{QEQ}} - \tilde{\mu}_m N_{\text{QEQ}}^m, \end{aligned} \quad (85)$$

holds, the differentiations with respect to \tilde{T} and $\tilde{\mu}$ lead to

$$\begin{aligned} \Sigma_{\text{QEQ}}(X) &= -\frac{\partial \Phi[\tilde{T}, \tilde{\mu}; \Omega_{\text{QEQ}}, X]}{\partial \tilde{T}}, \\ N_{\text{QEQ}}^m(X) &= -\frac{\partial \Phi[\tilde{T}, \tilde{\mu}; \Omega_{\text{QEQ}}, X]}{\partial \tilde{\mu}_m}, \end{aligned} \quad (86)$$

where we note that the implicit differentiations of Eq. (85) with respect to E_{QEQ} and N_{QEQ} vanish, due to the critical equations for the variational forms, Eqs. (82) and (83); also we denote $\Sigma_{\text{QEQ}}(X) = \Sigma[E_{\text{QEQ}}, \Omega_{\text{QEQ}}, N_{\text{QEQ}}, X]$. Finally, by substituting Eq. (86) into Eq. (85), we obtain

$$\begin{aligned} E_{\text{QEQ}}(X) &= \Phi[\tilde{T}, \tilde{\mu}; \Omega_{\text{QEQ}}, X] - \tilde{T} \frac{\partial \Phi[\tilde{T}, \tilde{\mu}; \Omega_{\text{QEQ}}, X]}{\partial \tilde{T}} \\ &\quad - \tilde{\mu}_m \frac{\partial \Phi[\tilde{T}, \tilde{\mu}; \Omega_{\text{QEQ}}, X]}{\partial \tilde{\mu}_m}. \end{aligned} \quad (87)$$

Next, by employing the above results for the fast dynamics, we derive the effective slow dynamics, which is the reaction dynamics. The time evolutions of the internal energy $E(t)$, the volume $\Omega(t)$ and the number of the open chemicals $N(t)$ for the reaction dynamics are already solved, by using the time evolution of the confined chemicals $X(t)$ and Eqs. (86) and (87), as

$$E = E_{\text{QEQ}}(X), \Omega = \Omega_{\text{QEQ}}(X), N = N_{\text{QEQ}}(X). \quad (88)$$

Substituting these evolutions into Eq. (3) and taking Eq. (4) into account, we obtain the effective slow dynamics as

$$\begin{aligned} \frac{dX^i}{dt} &= S_r^i J^r(t), \quad \frac{d\tilde{E}}{dt} = -\frac{dE_{\text{QEQ}}(X)}{dt}, \\ \frac{d\tilde{\Omega}}{dt} &= -\frac{d\Omega_{\text{QEQ}}(X)}{dt}, \quad \frac{d\tilde{N}^m}{dt} = O_r^m J^r(t) - \frac{dN_{\text{QEQ}}^m(X)}{dt}, \end{aligned} \quad (89)$$

which is Eq. (17) in the main text.

Before closing this appendix, we comment on the extensive variables in the reservoir at the quasi-equilibrium state, $(\tilde{E}_{\text{QEQ}}, \tilde{\Omega}_{\text{QEQ}}, \tilde{N}_{\text{QEQ}})$. Since $(\Delta_E)_{\text{QEQ}} = E_{\text{QEQ}} - E_0$, $(\Delta_\Omega)_{\text{QEQ}} = \Omega_{\text{QEQ}} - \Omega_0$, and $(\Delta_N)_{\text{QEQ}} = N_{\text{QEQ}} - N_0$, we get, from Eq. (78),

$$\begin{aligned} \tilde{E}_{\text{QEQ}}(X) &= \tilde{E}_0 - \{E_{\text{QEQ}}(X) - E_0\} \\ \tilde{\Omega}_{\text{QEQ}}(X) &= \tilde{\Omega}_0 - \{\Omega_{\text{QEQ}}(X) - \Omega_0\} \\ \tilde{N}_{\text{QEQ}}^m(X) &= \tilde{N}_0^m - \{N_{\text{QEQ}}^m(X) - N_0^m\}. \end{aligned} \quad (90)$$

If we set an initial condition for the confined chemicals to X_0 , the initial condition for the other variables in Eq. (89), $(\tilde{E}(0), \tilde{\Omega}(0), \tilde{N}(0))$, is given by Eq. (90) with $X = X_0$.

Appendix C

In this appendix, for a given X , we prove the uniqueness of the volume $\Omega(X)$, which is given by

$$\Omega(X) = \arg \min_{\Omega} \left\{ \Omega \varphi \left(\frac{X}{\Omega} \right) + \tilde{\Pi} \Omega \right\}. \quad (91)$$

The critical equation for this variational form is

$$h(\Omega) := \varphi \left(\frac{X}{\Omega} \right) - \frac{X^i}{\Omega} \partial_i \varphi \left(\frac{X}{\Omega} \right) + \tilde{\Pi} = 0, \quad (92)$$

where $\partial_i \varphi(X/\Omega) = \partial \varphi(x) / \partial x^i |_{x=X/\Omega}$ and we have defined the function $h(\Omega)$. The differentiation of $h(\Omega)$ is given as

$$\frac{dh}{d\Omega} = \Omega^{-3} X^i \left[\partial_i \partial_j \varphi \left(\frac{X}{\Omega} \right) \right] X^j. \quad (93)$$

Since φ is strictly convex, its Hessian $\partial_i \partial_j \varphi$ is positive definite. Thus, the function $h(\Omega)$ is a strictly increasing function for $\Omega > 0$. Accordingly, the critical equation, Eq. (92) has a unique solution for Ω . Therefore, the volume $\Omega(X)$ is uniquely determined by a given X .

Appendix D

In this appendix, we show that the intersection,

$$\mathfrak{R}^{\mathcal{Y}}(\tilde{\Pi}, \tilde{\mu}) = \mathcal{I}^{\mathcal{Y}}(\tilde{\Pi}, \tilde{\mu}) \cap \mathcal{Z}^{\mathcal{Y}}(\tilde{\mu}), \quad (94)$$

exists only when $\tilde{\Pi} < \varphi^*(y^{\text{EQ}})$. Since the Bregman divergence $\mathcal{D}^{\mathcal{Y}}[y^{\text{EQ}}||y]$ in Eq. (44) represents the deviation at the point y^{EQ} between the convex function $\varphi^*(y^{\text{EQ}})$ and tangent plane at the point y , a point y' exists in \mathcal{Y} such that $\varphi^*(y^{\text{EQ}}) - \varphi^*(y') - \mathcal{D}^{\mathcal{Y}}[y^{\text{EQ}}||y'] > 0$. Consider the set of all such points, that is the region $\mathcal{Z}^{\mathcal{Y}}(\tilde{\mu})$, which is unbounded and convex. Since y^{EQ} is on the boundary of $\mathcal{Z}^{\mathcal{Y}}(\tilde{\mu})$, the region $\mathcal{Z}^{\mathcal{Y}}(\tilde{\mu})$ lies inside in the sublevel set $\{y | \varphi^*(y) < \varphi^*(y^{\text{EQ}})\}$, which is bounded by $\mathcal{I}^{\mathcal{Y}}(\varphi^*(y^{\text{EQ}}), \tilde{\mu})$ as shown in FIG. 9.

If $\tilde{\Pi} \geq \varphi^*(y^{\text{EQ}})$, then $\mathcal{I}^{\mathcal{Y}}(\tilde{\Pi}, \tilde{\mu})$ lies outside the sublevel set $\{y | \varphi^*(y) < \varphi^*(y^{\text{EQ}})\}$ and therefore outside of $\mathcal{Z}^{\mathcal{Y}}(\tilde{\mu})$, i.e. there is no intersection.

If $\tilde{\Pi} < \varphi^*(y^{\text{EQ}})$, then $\mathcal{I}^{\mathcal{Y}}(\tilde{\Pi}, \tilde{\mu})$ lies inside the sublevel set $\{y | \varphi^*(y) < \varphi^*(y^{\text{EQ}})\}$, and due to the unboundedness and convexity of $\mathcal{Z}^{\mathcal{Y}}(\tilde{\mu})$, the intersection exists.

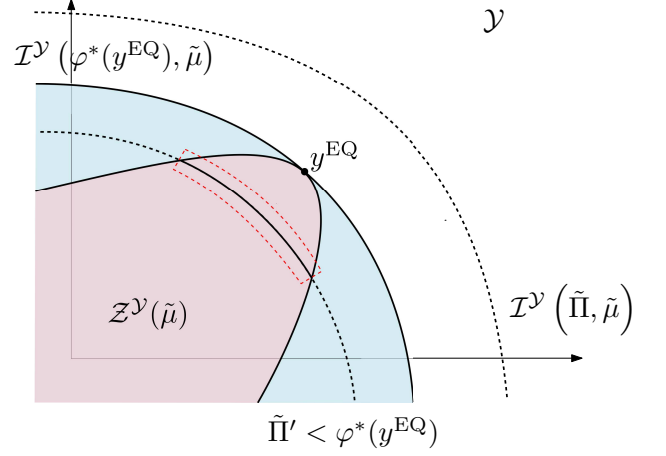


FIG. 9. Illustration of the proof for the existence of the intersection $\mathcal{I}^{\mathcal{Y}}(\tilde{\Pi}, \tilde{\mu}) \cap \mathcal{Z}^{\mathcal{Y}}(\tilde{\mu})$. The region $\mathcal{Z}^{\mathcal{Y}}(\tilde{\mu})$ is shown by light purple color. The sublevel set $\{y | \varphi^*(y) < \varphi^*(y^{\text{EQ}})\}$, indicated by blue color, is bounded by the level hypersurface $\mathcal{I}^{\mathcal{Y}}(\varphi^*(y^{\text{EQ}}), \tilde{\mu})$ (solid curve). Moreover, the boundary of $\mathcal{Z}^{\mathcal{Y}}(\tilde{\mu})$ intersects $\mathcal{I}^{\mathcal{Y}}(\varphi^*(y^{\text{EQ}}), \tilde{\mu})$ in exactly one point, namely y^{EQ} . If $\tilde{\Pi} \geq \varphi^*(y^{\text{EQ}})$, the hypersurface $\mathcal{I}^{\mathcal{Y}}(\tilde{\Pi}, \tilde{\mu})$ (outer dashed curve) has no intersection with $\mathcal{Z}^{\mathcal{Y}}(\tilde{\mu})$, whereas for $\tilde{\Pi} < \varphi^*(y^{\text{EQ}})$, the hypersurface $\mathcal{I}^{\mathcal{Y}}(\tilde{\Pi}', \tilde{\mu})$ (inner dashed curve) must have the intersection with $\mathcal{Z}^{\mathcal{Y}}(\tilde{\mu})$. The intersection is indicated by the solid black curve inside the curved red rectangle.

Appendix E

In the slow dynamics, the system is always in the quasi-equilibrium state, and therefore the number of open chemicals $N(X)$ can be evaluated in Eq. (20) as

$$N^m(X) = - \frac{\partial \Phi[\tilde{T}, \tilde{\mu}; \Omega(X), X]}{\partial \tilde{\mu}_m}. \quad (95)$$

Dividing both sides of this equation by $\Omega(X)$ yields

$$\begin{aligned} n^m(X) &= \frac{N^m(X)}{\Omega(X)} = \frac{\partial \varphi[\tilde{T}, \tilde{\mu}; X/\Omega(X)]}{\partial \tilde{\mu}_m}, \\ &= e^{\{\tilde{\mu}_m - \mu_m^o(\tilde{T})\}/R\tilde{T}} = \tilde{n}^m \end{aligned} \quad (96)$$

where we use the homogeneity of the partial grand potential $\Phi[\tilde{T}, \tilde{\mu}; \Omega, X]$.

* These two authors contributed equally.

† E-mail me at: tetsuya@mail.crmind.net

- [1] J. von Neumann and A. W. Burks, *Theory of Self-Replicating Automata*, (University of Illinois Press, Urbana, IL, 1966).
- [2] R. A. Freitas Jr. and R. C. Merkle, *Kinematic Self-Replicating Machines*, (Landes Bioscience, Georgetown, TX, 2004).

- [3] M. Pekař, *Non-Equilibrium Thermodynamics View on Kinetics of Autocatalytic Reactions – Two illustrative Examples*, *Molecules*, **26(3)**, 585 (2021).
- [4] H. Dourado and M. J. Lercher, *An Analytical Theory of Balanced Cellular Growth*, *Nat. Commun.*, **11**, 1226 (2020).
- [5] W. Lin, E. Kussell, L. Young and C. Jacobs-Wagner, *Origin of Exponential Growth in Nonlinear Reaction Networks*, *Proc. Natl. Acad. Sci. USA*, **117(45)**, 27795 (2020).
- [6] P. Thomas, G. Terradot, V. Danos and A. Y. Weiße, *Sources, Propagation and Consequences of Stochasticity in Cellular Growth*, *Nat. Commun.*, **9**, 4528 (2018).
- [7] Y. Liu and D. J. T. Sumpter, *Mathematical Modeling Reveals Spontaneous Emergence of Self-replication in Chemical Reaction Systems*, *J. Biol. Chem.* **293(49)**, 18854 (2018).
- [8] C. Furusawa and K. Kaneko, *Formation of Dormant Mode by Evolution in Biological Systems*, *Phys. Rev. E*, **97**, 042410 (2018).
- [9] D. Andrieux and P. Gaspard, *Nonequilibrium Generation of Information in Copolymerization Processes*, *Proc. Natl. Acad. Sci. USA*, **105(28)**, 9516 (2008).
- [10] A. Roy, D. Goberman and R. Pugatch, *A Unifying Autocatalytic Network-based Framework for Bacterial Growth Laws*, *Proc. Natl. Acad. Sci. USA*, **118(33)**, e2107829118 (2021).
- [11] P. P. Pandey and S. Jain, *Analytical Derivation of Bacterial Growth Law from a Simple Model of Intracellular Chemical Dynamics*, *Theory Biosci.* **135**, 121 (2016).
- [12] A. Maitra and K. A. Dill, *Bacterial Growth Laws Reflect the Evolutionary Importance of Energy Efficiency*, *Proc. Natl. Acad. Sci. USA*, **112(2)**, 406 (2015).
- [13] G. F. Joyce and J. W. Szostak, *Protocells and RNA Self-Replication*, *Cold Spring Harb. Perspect. Biol.* **10**, a034801 (2018).
- [14] R. Serra and M. Villani, *Modelling Protocells: The Emergent Synchronization of Reproduction and Molecular Replication*, (Springer, Berlin, 2017).
- [15] K. Kurihara, et al., *A Recursive Vesicle-based Model Protocell with a Primitive Model Cell Cycle*, *Nat. Commun.* **6**, 8352 (2015).
- [16] K. Ruiz-Mirazo, C. Briones and A. de la Escosura, *Prebiotic Systems Chemistry: New Perspectives for the Origins of Life*, *Chem. Rev.* **114**, 285 (2014).
- [17] Y. Himeoka and K. Kaneko, *Entropy Production of a Steady-growth Cell with Catalytic Reactions*, *Phys. Rev. E* **90**, 042714 (2014).
- [18] N. Ichihashi, et al., *Darwinian Evolution in a Translation-Coupled RNA Replication System within a Cell-like Compartment*, *Nat. Comm.* **4**, 2494 (2013).
- [19] F. Mavelli and K. Ruiz-Mirazo, *Theoretical Conditions for the Stationary Reproduction of Model Protocells*, *Integr. Biol.* **5**, 324 (2013).
- [20] V. Noireaux, Y. T. Maeda and A. Libchaber, *Development of an Artificial cell, from Self-organization to Computation and Self-reproduction*, *Proc. Natl. Acad. Sci. USA*, **108(9)**, 3473 (2011).
- [21] K. Kurihara, et al., *Self-reproduction of Supramolecular Giant Vesicles Combined with the Amplification of Encapsulated DNA*, *Nat. Chem.* **3**, 775 (2011).
- [22] H. Kita, et al. *Replication of Genetic Information with Self-Encoded Replicase in Liposomes*, *ChemBioChem.* **9**, 2403 (2008).
- [23] S. Rasmussen, et al., *Protocells: Bridging Nonliving and Living Matter* (The MIT Press, Cambridge, MA, 2008)
- [24] D. Segré, D. Ben-Eli and D. Lancet, *Compositional Genomes: Prebiotic Information Transfer in Mutually Catalytic Noncovalent Assemblies*, *Proc. Natl. Acad. Sci. USA*, **97(8)**, 4112 (2000).
- [25] J. Unterberger and P. Nghe, *Stoichiometric and Dynamical Autocatalysis for Diluted Chemical Reaction Networks*, arXiv:2109.01130 (2021).
- [26] A. Blokhuis, D. Lacoste and P. Nghe, *Universal Motifs and the Diversity of Autocatalytic Systems*, *Proc. Natl. Acad. Sci. USA*, **117(41)**, 25230 (2020).
- [27] M. Steel, W. Hordijk and J. C. Xavier, *Autocatalytic Networks in Biology: Structural Theory and Algorithms*, *J. R. Soc. Interface*, **16**, 20180808 (2019).
- [28] U. Barenholz, et al., *Design Principles of Autocatalytic Cycles Constrain Enzyme Kinetics and Force Low Substrate Saturation at Flux Branch Points*, *eLife*, **6**, e20667 (2017).
- [29] S. Jain and S. Krishna, *Autocatalytic Sets and the Growth of Complexity in an Evolutionary Model*, *Phys. Rev. Lett.* **81(25)**, 5684 (1998).
- [30] S. A. Kauffman, *Autocatalytic Sets of Proteins*, *J. Theor. Biol.* **119(1)**, 1 (1986).
- [31] M. Eigen and P. Schuster, *The Hypercycle A Principle of Natural Self-Organization* (Springer, Berlin, 1979)
- [32] M. Scott, C. W. Gunderson, E. M. Mateescu, Z. Zhang and T. Hwa, *Interdependence of Cell Growth and Gene Expression: Origins and Consequences*, *Science*, **330(6007)**, 1099 (2010).
- [33] S. Kostinski and S. Reuveni, *Growth Laws and Invariants from Ribosome Biogenesis in Lower Eukarya*, *Phys. Rev. Res.* **3**, 013020 (2021).
- [34] S. Kostinski and S. Reuveni, *Ribosome Composition Maximizes Cellular Growth Rates in E. coli*, *Phys. Rev. Lett.* **125**, 028103 (2020).
- [35] S. Jun, F. Si, R. Pugatch and M. Scott, *Fundamental Principles in Bacterial Physiology—History, Recent Progress, and the Future with Focus on Cell Size Control: a Review*, *Rep. Prog. Phys.* **81** 056601 (2018).
- [36] S. Reuvani, M. Ehrenberg and J. Paulsson, *Ribosomes are Optimized for Autocatalytic production*, *Nature*, **547**, 293 (2017).
- [37] M. Scott, S. Klumpp, E. M. Mateescu and T. Hwa, *Emergence of Robust Growth Laws from Optimal Regulation of Ribosome Synthesis*, *Mol. Syst. Biol.* **10**, 747 (2014).
- [38] M. Scott and T. Hwa, *Bacterial Growth Laws and Their Applications*, *Curr. Opin. Biotechnol.* **22**, 559 (2011).
- [39] S. Müller, D. Széliová and J. Zanghellini, *Elementary Vectors and Autocatalytic Sets for Computational Models of Cellular Growth*, bioRxiv, doi:10.1101/2021.10.31.466640 (2021).
- [40] S. Müller, *Elementary Growth Modes/Vectors and Minimal Autocatalytic Sets for Kinetic/Constraint-based Models of Cellular Growth*, bioRxiv, doi:10.1101/2021.02.24.432769 (2021).
- [41] D. H. de Groot, J. Hulshof, B. Teusink, F. J. Bruggeman and R. Planqué, *Elementary Growth Modes Provide a Molecular Description of Cellular Self-fabrication*, *PLoS Comput. Biol.* **16(1)**, e1007559 (2020).
- [42] H. de Jong, et al., *Mathematical Modelling of Microbes: Metabolism, Gene Expression and Growth*, *J. R. Soc. Interface* **14**, 20170502 (2017).

- [43] R. Rao and M. Esposito, *Nonequilibrium Thermodynamics of Chemical Reaction Networks: Wisdom from Stochastic Thermodynamics*, Phys. Rev. X **6**, 041064 (2016).
- [44] M. Polettini and M. Esposito, *Irreversible Thermodynamics of Open Chemical Networks. I. Emergent Cycles and Broken Conservation Laws*, J. Chem. Phys. **141**, 024117 (2014).
- [45] H. Ge and H. Qian, *Nonequilibrium Thermodynamic Formalism of Nonlinear Chemical Reaction Systems with Waage–Guldberg’s Law of Mass Action*, Chem. Phys. **472**, 241 (2016).
- [46] H. Qian and T. C. Reluga, *Nonequilibrium Thermodynamics and Nonlinear Kinetics in a Cellular Signaling Switch*, Phys. Rev. Lett. **94**, 028101 (2005).
- [47] G. Craciun, S. Müller, C. Pantea and P. Y. Yu, *A Generalization of Birch’s Theorem and Vertex-Balanced Steady States for Generalized Mass-action Systems*, Math. Biosci. Eng. **16**, 8243 (2019).
- [48] M. P. Millán, A. Dickenstein, A. Shiu and C. Conradi, *Chemical Reaction Systems with Toric Steady States*, Bull. Math. Biol. **74**, 1027 (2012).
- [49] G. Craciun, A. Dickenstein, A. Shiu and B. Sturmfels, *Toric Dynamical Systems*, J. Symb. Comput. **44**, 1551 (2009).
- [50] F. Horn and R. Jackson, *General Mass Action Kinetics*, Arch. Ration. Mech. Anal. **47**, 81 (1972).
- [51] Y. Sughiyama, D. Loutchko, A. Kamimura and T. J. Kobayashi, *A Hessian Geometric Structure of Chemical Thermodynamic Systems with Stoichiometric Constraints*, arXiv:2112.12403 (2021).
- [52] T. J. Kobayashi, D. Loutchko, A. Kamimura and Y. Sughiyama, *Kinetic Derivation of the Hessian Geometric Structure in Chemical Reaction Systems*, arXiv:2112.14910 (2021).
- [53] H. B. Callen, *Thermodynamics and an Introduction to Thermostatistics*, 2nd ed. (John Wiley & Sons, New York, 1985).
- [54] D. Kondepudi and I. Prigogine, *Modern Thermodynamics*, (John Wiley & Sons, New York, 1998).
- [55] H. Shima, *The Geometry of Hessian Structures*, (World Scientific Pub. Co. Inc., Singapore, 2007).
- [56] S. Amari and H. Nagaoka, *Methods of Information Geometry*, (Oxford University Press, 1993).
- [57] L. Bregman, *The Relaxation Method of Finding the Common Point of Convex Sets and Its Application to the Solution of Problems in Convex Programming*, USSR Comput. Math. Math. Phys. **7**, 200 (1967).
- [58] D. A. Beard and H. Qian, *Chemical Biophysics*, (Cambridge University Press, Cambridge, 2008).
- [59] To be more precise, the functional forms of the reaction fluxes $J(t)$ must be chosen so that $\Sigma^{\text{tot}}(X(t))$ becomes an increasing function with respect to time t .
- [60] A ray τ in \mathfrak{X} can be expressed as follows: for a representative $X_\tau \in \mathfrak{X}$, write $\tau = \{X|X^i = \alpha X_\tau^i, \alpha > 0\}$.
- [61] Since $\rho_{\mathfrak{X}}(X) \neq \rho_{\mathfrak{X}}(X')$ for any two points $X \in \tau$ and $X' \in \tau'$ ($\tau \neq \tau'$), the map $\bar{\rho}_{\mathfrak{X}} : \mathcal{P}\mathfrak{X} \rightarrow \mathfrak{X}$ is injective.
- [62] The standard density x_o satisfies $\partial_i \varphi(x_o) = \nu_o(\tilde{T}) + R\tilde{T} \log x_o^i = 0$, which means that x_o is the density that sets the corresponding chemical potential to zero.
- [63] A. L. Koch, *Microbial Physiology and Ecology of Slow Growth*, Microbiology and Molecular Biology Reviews **61(3)**, 305 (1997)
- [64] O. Gefen, O. Fridman, I. Ronin and N. Q. Balaban, *Direct Observation of Single Stationary-phase Bacteria Reveals a Surprisingly Long Period of Constant Protein Production Activity*, Proc. Natl. Acad. Sci. USA, **111(1)**, 556 (2014)
- [65] M. Bergkessel, D. W. Basta and D. K. Newman *The Physiology of Growth Arrest: Uniting Molecular and Environmental Microbiology*, Nat. Rev. Microbiol. **14**, 549 (2016)
- [66] Y. Himeoka and K. Kaneko, *Theory for Transitions Between Exponential and Stationary Phases: Universal Laws for Lag Time*, Phys. Rev. X, **7(2)**, 021049 (2017)